NASA TECHNICAL MEMORANDUM

NASA TM X-2762

NASA TM X-2762

LOW-SUBSONIC AERODYNAMIC CHARACTERISTICS OF A 60° SWEPT DELTA-WING SPACE SHUTTLE ORBITER

by Delma C. Freeman, Jr.

Langley Research Center
Hampton, Va. 23665

NATIONAL AERONAUTICS AND SPACE ADMINISTRATION • WASHINGTON, D. C. • JULY 1973

1. Report No.	2. Government Accession No.	3. Recipient's Catalog No.
NASA TM X-2762		

4. Title and Subtitle	5. Report Date
LOW-SUBSONIC AERODYNAMIC CHARACTERISTICS OF A 60° SWEPT DELTA-WING SPACE SHUTTLE ORBITER	July 1973
	6. Performing Organization Code

7. Author(s)	8. Performing Organization Report No.
Delma C. Freeman, Jr.	L-8722
	10. Work Unit No.
9. Performing Organization Name and Address	502-37-01-01
NASA Langley Research Center Hampton, Va. 23665	11. Contract or Grant No.
	13. Type of Report and Period Covered
12. Sponsoring Agency Name and Address	Technical Memorandum
National Aeronautics and Space Administration Washington, D.C. 20546	14. Sponsoring Agency Code

15. Supplementary Notes

16. Abstract

An investigation has been conducted in the Langley low-turbulence pressure tunnel to determine Reynolds number effects on the low-subsonic aerodynamic characteristics and longitudinal control effectiveness of a North American Rockwell phase B delta-wing orbiter concept designated 134D. The model was tested over a range of Reynolds numbers, based on body length, from 5.25×10^6 to 29.40×10^6, at Mach numbers less than 0.35, at angles of attack from approximately -2° to 28°, and at angles of sideslip of 0° and -6°.

17. Key Words (Suggested by Author(s))	18. Distribution Statement
Reynolds number effects Low-subsonic aerodynamic characteristics of entry vehicles Space shuttle orbiter	Unclassified – Unlimited

19. Security Classif. (of this report)	20. Security Classif. (of this page)	21. No. of Pages	22. Price*
Unclassified	Unclassified	55	$3.00

*For sale by the National Technical Information Service, Springfield, Virginia 22151

LOW-SUBSONIC AERODYNAMIC CHARACTERISTICS OF A 60° SWEPT DELTA-WING SPACE SHUTTLE ORBITER

By Delma C. Freeman, Jr.
Langley Research Center

SUMMARY

An investigation has been conducted in the Langley low-turbulence pressure tunnel to determine the low-subsonic longitudinal and lateral-directional aerodynamic characteristics and longitudinal control effectiveness of a North American Rockwell phase B delta-wing orbiter concept designated 134D. The model was tested with and without fixed transition over a range of Reynolds numbers, based on body length, from 5.25×10^6 to 29.40×10^6, at Mach numbers less than 0.35, at angles of attack from approximately -2° to 28°, and at angles of sideslip of 0° and -6°.

The results of the investigation showed that the model exhibited static longitudinal stability up to an angle of attack of 15° with sufficient elevon effectiveness to trim up to an angle of attack of 22° with relatively small Reynolds number effects except on the maximum lift-drag ratio, which was increased by 0.8 from the lowest to the highest test Reynolds numbers. Increasing the Reynolds number, based on body length, from 5.25×10^6 to 29.40×10^6 resulted in a large increase in the directional-stability parameter and a large decrease in the effective-dihedral parameter between angles of attack of 16° and 22°.

INTRODUCTION

One of the current goals of the National Aeronautics and Space Administration is the development of an economical space transportation system capable of transporting large payloads to and from near-earth orbit. As part of this general effort, wind-tunnel tests of a North American Rockwell phase B delta-wing orbiter concept designated 134D (see ref. 1) have been conducted over the entire entry to landing speed range at the Langley Research Center. The investigation reported herein was conducted in the Langley low-turbulence pressure tunnel to determine the basic low-subsonic longitudinal and lateral-directional aerodynamic characteristics and longitudinal control effectiveness of the model. The model was tested with and without fixed transition over a range of Reynolds numbers, based on body length, from 5.25×10^6 to 29.40×10^6, at Mach numbers less than

0.35, at angles of attack from approximately -2^{o} to 28^{o}, and at angles of sideslip of 0^{o} and -6^{o}. Some preliminary results were presented in references 2 and 3.

SYMBOLS

The longitudinal data are referred to the stability system of axes and the lateral-directional data are referred to the body system of axes. (See fig. 1.) The moment center was located at 67.1 percent body length, as presented in figure 2.

The units used for the physical quantities of this paper are given both in the International System of Units (SI) and in the U.S. Customary Units. Measurements and calculations were made in U.S. Customary Units. The equivalent values of units were determined by using the conversion factors given in reference 4.

A aspect ratio

b wing span, m (ft)

$\bar{c}$ mean aerodynamic chord, m (ft)

C_A total axial-force coefficient, $\frac{-F_X}{q_\infty S}$

C_D drag coefficient, $\frac{\text{Drag}}{q_\infty S}$

$C_{D,corr}$ forebody drag coefficient (corrected to correspond to a base pressure equal to free-stream static pressure)

$C_{D,o}$ drag coefficient at $C_L = 0$

C_L lift coefficient, $\frac{\text{Lift}}{q_\infty S}$

C_{L_α} lift-curve slope

C_l rolling-moment coefficient, $\frac{M_X}{q_\infty S\bar{c}}$

$C_{l_\beta} = \frac{\Delta C_l}{\Delta\beta}$, per deg (where $\beta = -6^{o}$ and 0^{o})

C_m pitching-moment coefficient, $\frac{M_Y}{q_\infty S\bar{c}}$

C_N normal-force coefficient, $\frac{-F_Z}{q_\infty S}$

C_n yawing-moment coefficient, $\frac{M_Z}{q_\infty Sb}$

$C_{n_\beta} = \frac{\Delta C_n}{\Delta \beta}$, per deg (where $\beta = -6^o$ and 0^o)

$C_{n_{\beta,dyn}} = C_{n_\beta} - \frac{I_Z}{I_X} C_{l_\beta} \sin \alpha$

$C_{p,b}$ base pressure coefficient, $\frac{p_b - p_\infty}{q_\infty}$ (see fig. 2 for definition of subscripts 1 and 2)

$C_{p,c}$ balance cavity pressure coefficient, $\frac{p_c - p_\infty}{q_\infty}$

C_Y lateral-force coefficient, $\frac{F_Y}{q_\infty S}$

$C_{Y_\beta} = \frac{\Delta C_Y}{\Delta \beta}$, per deg (where $\beta = -6^o$ and 0^o)

D drag

F_X axial force, N (lb)

F_Y lateral force, N (lb)

F_Z normal force, N (lb)

I_X moment of inertia about longitudinal body axis, kg-m^2 (slug-ft^2)

I_Z moment of inertia about normal body axis, kg-m^2 (slug-ft^2)

L lift, N (lb)

L/D lift-drag ratio

$(L/D)_{corr}$ lift-drag ratio computed using $C_{D,corr}$

l body length, m (ft)

M_X	rolling moment, m-N (in-lb)
M_Y	pitching moment, m-N (in-lb)
M_Z	yawing moment, m-N (in-lb)
p_b	static pressure at base of model, N/m^2 (lb/ft^2)
p_c	cavity pressure, N/m^2 (lb/ft^2)
p_∞	free-stream static pressure, N/m^2 (lb/ft^2)
q_∞	free-stream dynamic pressure, N/m^2 (lb/ft^2)
R	Reynolds number, based on body length
S	reference wing area, m^2 (ft^2)
S_e	elevon area, m^2 (ft^2)
s	leading-edge suction parameter, percent
X,Y,Z	body reference axes
α	angle of attack, deg
β	angle of sideslip, deg
δ_e	elevon deflection, positive when trailing edge is down, deg
ψ	angle of yaw, deg

Subscripts:

corr	corrected
max	maximum
s	stability axes

trim at longitudinal trimmed conditions

Model components:

B body

W wing

V_1 vertical tail

Z orbital maneuvering system pod (see fig. 2)

DESCRIPTION OF MODEL

The model tested was an 0.0118-scale model of a conceptual high-cross-range shuttle orbiter (the North American Rockwell phase B delta-wing orbiter concept designated 134D). The general arrangement of the model is shown in figure 2. A photograph of the model is presented in figure 3. The model had a leading-edge wing sweep of 60° and elevon surfaces ($S_e/S = 0.065$) that served both for pitch and roll control. The wing had an NACA 0009-64 airfoil section with 0° incidence at the root and an NACA 0012-64 airfoil section at the wing tip with -5° twist about the wing trailing edge. The rudder could be deflected for directional control or flared for speed-brake applications at transonic and supersonic speeds.

APPARATUS AND TESTS

The experimental results were obtained in the Langley low-turbulence pressure tunnel, which is a variable-pressure, single-return facility having a closed test section 0.914 meter (3.0 feet) wide and 2.282 meters (7.5 feet) high. This facility can accommodate tests in air at Reynolds numbers up to approximately 49.2×10^6 per meter (15.0×10^6 per foot) at Mach numbers up to about 0.40.

Tests were made at Reynolds numbers, based on body length, from 5.25×10^6 to 29.40×10^6 at Mach numbers up to 0.35. Angle of attack was varied from -2° to 28° at angles of sideslip of 0° and -6°. In order to assure turbulent flow at a fixed location on the model and thereby allow extrapolation of skin friction estimates to full-scale, some tests were made with fixed transition. Two different sizes of grit as determined by the methods of reference 5 were tested: 0.0073-cm grit sized to assure turbulent flow with minimum grit drag at a Reynolds number of 16×10^6 and 0.0124-cm grit sized to assure turbulent flow at a Reynolds number of 5×10^6. Transition was fixed on the aerodynamic

surfaces 1.27 cm aft streamwise of the leading edge and on the body 3.81 cm aft of the nose.

MEASUREMENTS AND CORRECTIONS

The drag coefficients presented represent gross drag in that base drag has not been subtracted. Base and balance cavity pressures measured during the tests are indicated in the final part of each of the basic data figures presented. Measurements were made in three different locations and these locations are shown in figure 2. The data have been corrected for blockage and lift interference by the methods of references 6 and 7. Angles of attack have been corrected for the effects of balance and sting deflection due to aerodynamic loads.

RESULTS AND DISCUSSION

Static Longitudinal Characteristics

Effect of Reynolds number.- Presented in figures 4 to 7 are the results of tests to determine the effect of Reynolds number on the static longitudinal characteristics of the model. The data presented in figures 4 and 5 were obtained with a smooth model (natural transition), and the data presented in figures 6 and 7 were obtained with fixed transition by using 0.0124-cm-grit and 0.0073-cm-grit sizes, respectively. These results are summarized in figure 8 by comparing the forebody drag coefficient at zero lift and the maximum lift-drag ratio computed using forebody drag coefficient through the Reynolds number range for the smooth model and two grit sizes. At a Reynolds number of approximately 17×10^6 based on body length, the values of $(L/D)_{corr,max}$ and $(C_{D,o})_{corr}$ indicate that supercritical Reynolds numbers have been achieved and any changes in these parameters above this Reynolds number are small and result from reductions in skin-friction drag. These comparisons show that by addition of the grit to the smooth model to assure turbulent flow conditions over the entire model, the level of $C_{D,o}$ at the lower Reynolds number is increased and gives values that would be expected from extrapolating the high Reynolds number data. This indicates that properly fixing transition produces skin-friction drag that can be scaled directly to full-scale, as has been shown in previous investigations. These differences between natural-transition and fixed-transition measurements at the lower Reynolds numbers (less than approximately 12×10^6) indicate a mixture of laminar and turbulent flow on the smooth model, with the flow becoming more turbulent as the Reynolds number increases. A comparison of the base-pressure data $(C_{p,b})_1$ (figs. 4(g) and 6(g)) indicates that at the lower Reynolds numbers there is laminar separation in the area of the model base for the smooth model. There are other small differences indicated by the data but these are within the accuracy of the drag measurements.

Presented in figure 9 is the leading-edge suction parameter s (as derived from the expression of ref. 8 with the assumption of elliptical lift distribution) computed at $(L/D)_{max}$ plotted against Reynolds number for the smooth model and model with the 0.0073-cm-size grit:

$$s = \frac{\frac{C_L^2}{C_{L_\alpha}} - \left(C_D - C_{D,o}\right)}{\frac{C_L^2}{C_{L_\alpha}} - \frac{C_L^2}{\pi A}} \times 100$$

Increasing the Reynolds number from 5.25×10^6 to 29.40×10^6 increased the leading-edge suction parameter for the smooth model from approximately 81 percent to 94 percent. This effect is considered relatively small but results in an increase in maximum untrimmed lift-drag ratio of about 0.8. The model with transition fixed with 0.0073-cm grit shows an increase in s from approximately 77 percent to 92 percent for the range of Reynolds numbers presented. These results agree reasonably well with the results of reference 1, which were obtained with the use of a very similar model of a smaller scale. Although figure 8 shows that proper transition fixing insures drag data which can be scaled to full-scale conditions, these data show that transition does not greatly affect leading-edge suction. In order to obtain proper values of suction (>90 percent, ref. 8), leading-edge Reynolds number has to be greater than can be measured on scale models in atmospheric tunnels. Therefore, the remainder of the presented data were measured for the smooth model at $R = 21.0 \times 10^6$. This value of Reynolds number insures turbulent flow conditions and leading-edge suction greater than 90 percent.

Basic longitudinal characteristics.- The basic longitudinal characteristics of the model are presented in figures 10 to 12. Figure 10 shows only slight changes in the aerodynamic characteristics at low values of α due to the addition of the vertical tail and orbital maneuvering system pod to the wing-body combination. The elevon effectiveness data are presented in figure 11 and show that the model is longitudinally stable in the angle-of-attack range up to about 15^o (center of gravity at 0.67ℓ) with a slight destabilizing break in the curve above an angle of attack of 15^o for the lower elevon deflections. This unstable break results from wing-tip separation, which is relieved as the elevons are deflected for trim. The model could be trimmed up to an angle of attack of approximately 22^o at the maximum elevon deflection investigated and was longitudinally stable at trim throughout this range. The values of $(L/D)_{trim}$ and $C_{L,trim}$ calculated by using the data of figure 11 are presented in figure 12. These results show a maximum trimmed lift-drag ratio of 6.8 at angles of attack of 10^o to 11^o with a trimmed lift coefficient of approximately 0.3.

Static Lateral-Directional Characteristics

Effect of Reynolds number.- The effect of Reynolds number on the static lateral-directional stability characteristics is presented in figure 13. Increasing the Reynolds number, based on body length, from 5.25×10^6 to 29.40×10^6 resulted in a large increase in C_{n_β} and a large decrease in the effective dihedral parameter $\left(-C_{l_\beta}\right)$ at angles of attack between 16° and 22°. These effects are probably caused by the weakening of the wing leading-edge vortex influence on the windward sides of the body and vertical tail and on the leading wing-tip separation as Reynolds number increased (see ref. 3). The dynamic directional-stability parameter $C_{n_{\beta,dyn}}$ (see ref. 9) computed by using the data presented in figure 13 and $I_Z/I_X = 7.98$ is presented in figure 14. The fact that the value of $C_{n_{\beta,dyn}}$ remained positive throughout the test angle-of-attack range indicates that aperiodic divergence would not occur. An interesting point to be made is that even though the previously discussed longitudinal data indicated that supercritical Reynolds numbers have been achieved, there were still effects of Reynolds number on the lateral-directional characteristics.

Effect of elevon deflection.- The data of figure 15 present the effect of elevon deflection on the static lateral-directional characteristics of the model. These results indicate a slight increase in C_{n_β} and an increase in negative C_{l_β} for the elevon deflection of -5.1°. These effects probably result from induced effects on the flow field over the wing, since the absence of any marked effect of control deflection on C_{Y_β} indicates that the body and vertical tail lateral loading are essentially unchanged.

Effect of vertical tail.- The data presented in figure 16 show the effect of the centerline vertical tail on the static lateral-directional characteristics of the model. Installation of the vertical tail resulted in the addition of a constant positive increment in C_{n_β} and a correspondingly constant negative increment in C_{l_β}. The fact that the relative shapes of the curves were essentially unchanged confirms that the loading on the vertical tail is not greatly influenced by the flow field of the wing-body.

SUMMARY OF RESULTS

An investigation has been conducted to determine the low-subsonic aerodynamic characteristics of a 0.0118-scale model of a North American Rockwell phase B delta-wing orbiter concept designated 134D. The results of these tests may be summarized as follows:

1. The effect of Reynolds number variation from 5.25×10^6 to 29.40×10^6 on the longitudinal aerodynamic characteristics of the model was relatively small except for an increase in the maximum lift-drag ratio of approximately 0.8.

2. The model could be trimmed up to an angle of attack of 22^o at the maximum elevon deflection of the investigation, and the model was longitudinally stable at trim throughout this range.

3. The model directional-stability and effective-dihedral parameters were sensitive to Reynolds number variation at angles of attack above 12^o. Increasing the Reynolds number, based on body length, from 5.25×10^6 to 29.40×10^6 resulted in a large increase in directional stability and a correspondingly large decrease in effective dihedral between angles of attack of 16^o and 22^o. These Reynolds number effects persisted at high values where longitudinal characteristics were essentially independent of Reynolds number.

Langley Research Center,
National Aeronautics and Space Administration,
Hampton, Va., May 8, 1973.

REFERENCES

1. Parrell, H.: An Experimental Investigation of the Effect of Reynolds Number on the Low Speed Aerodynamic Characteristics of a Delta Wing Space Shuttle Orbiter Concept at Angles of Attack to 45 Degrees. SD 71-158 (Contract NAS 9-10960), North American Rockwell Corp., Sept. 10, 1971.

2. Love, Eugene S.: Advanced Technology and the Space Shuttle (10th Von Kármán Lecture). AIAA Paper No. 73-31, Jan. 1973.

3. Freeman, Delma C., Jr.; and Ellison, James C.: Aerodynamic Studies of Delta-Wing Shuttle Orbiters. Pt. I – Low Speed. Vol. III of Space Shuttle Aerothermodynamics Technology Conference, NASA TM X-2508, 1972, pp. 785-801.

4. Mechtly, E. A.: The International System of Units – Physical Constants and Conversion Factors (Revised). NASA SP-7012, 1969.

5. Braslow, Albert L.; Hicks, Raymond M.; and Harris, Roy V., Jr.: Use of Grit-Type Boundary-Layer-Transition Trips on Wind-Tunnel Models. NASA TN D-3579, 1966.

6. Herriot, John G.: Blockage Corrections for Three-Dimensional-Flow Closed-Throat Wind Tunnels, With Consideration of the Effect of Compressibility. NACA Rep. 995, 1950. (Supersedes NACA RM A7B28.)

7. Garner, H. C.; Rogers, E. W. E.; Acum, W. E. A.; and Maskell, E. C.: Subsonic Wind Tunnel Wall Corrections. AGARDograph 109, Oct. 1966.

8. Henderson, William P.: Studies of Various Factors Affecting Drag Due to Lift at Subsonic Speeds. NASA TN D-3584, 1966.

9. Moul, Martin T.; and Paulson, John W.: Dynamic Lateral Behavior of High-Performance Aircraft. NACA RM L58E16, 1958.

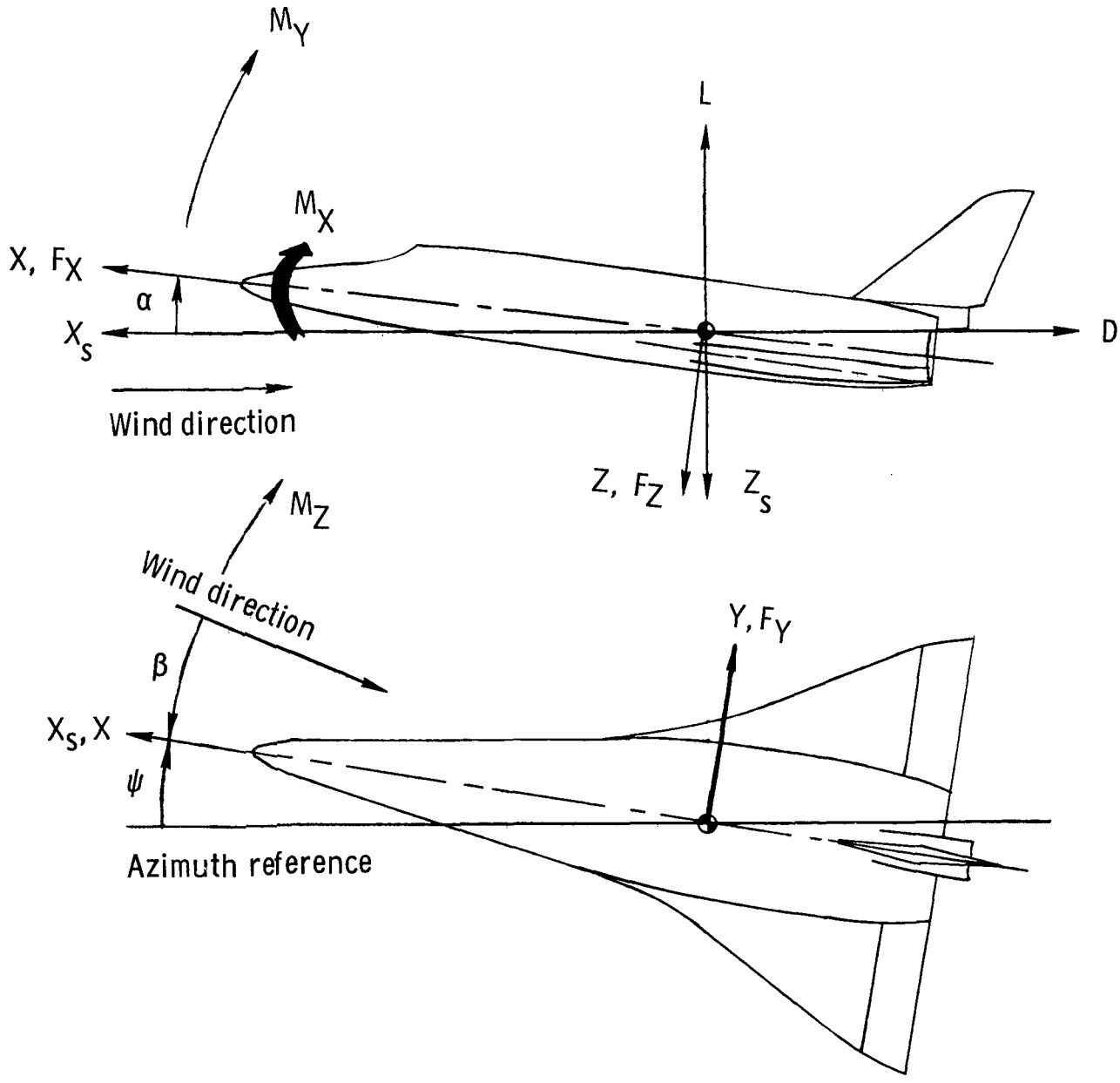

Figure 1.- System of axes used in investigation. Arrows indicate positive directions of moments, forces, and angles.

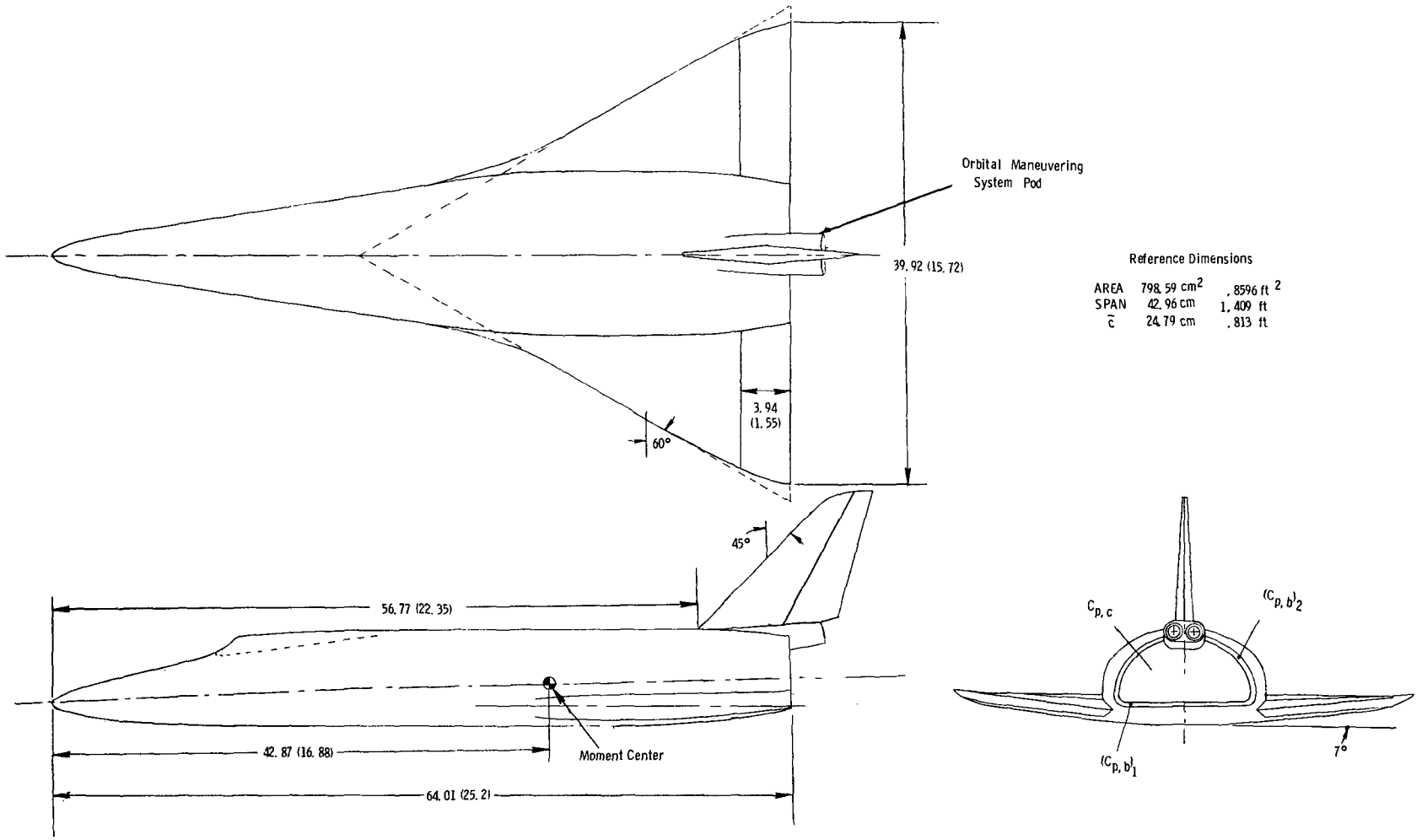

Figure 2.- Three-view drawing of model used in investigation. All dimensions are in centimeters with inches given in parentheses.

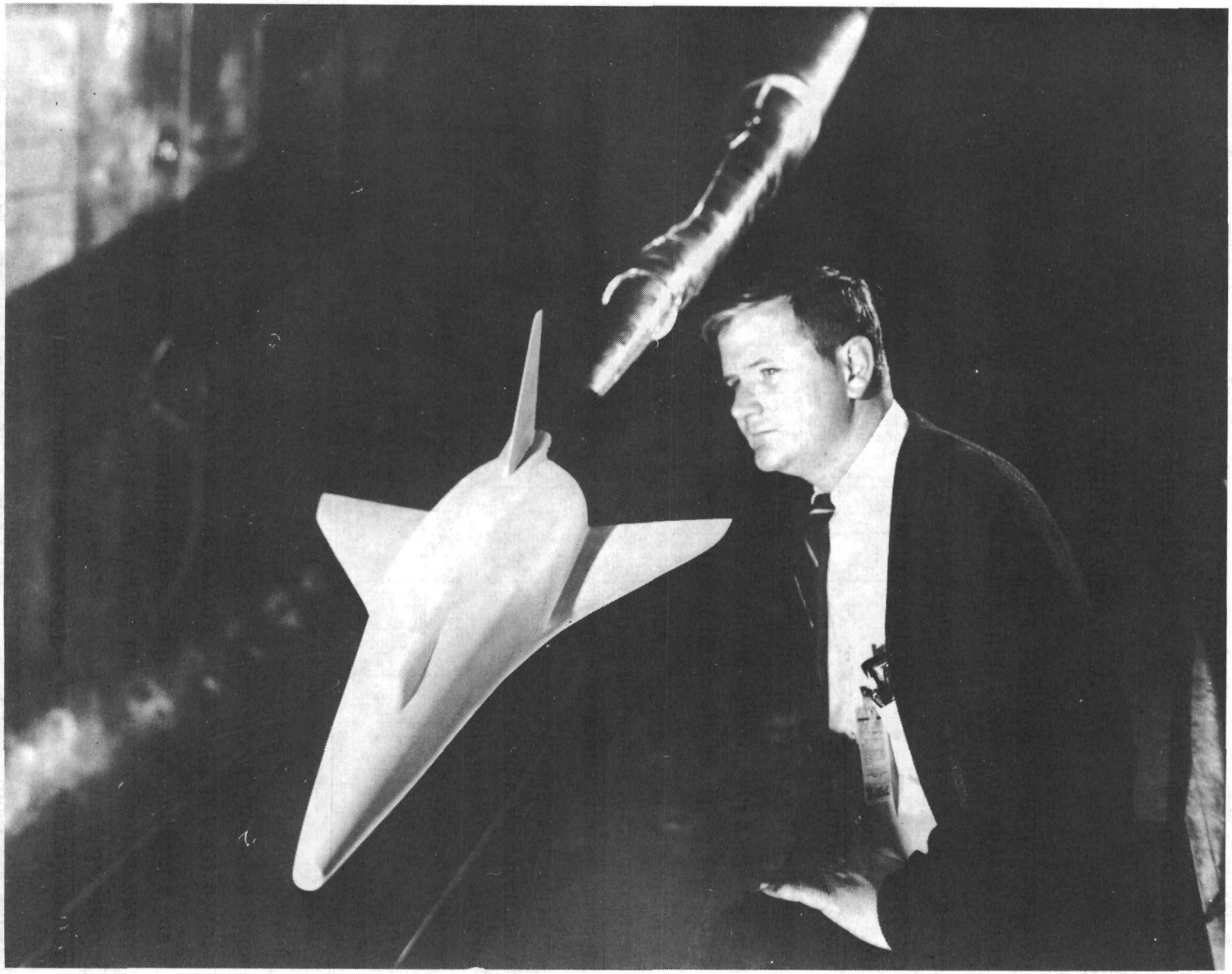

L-71-3808

Figure 3.- Photograph of model.

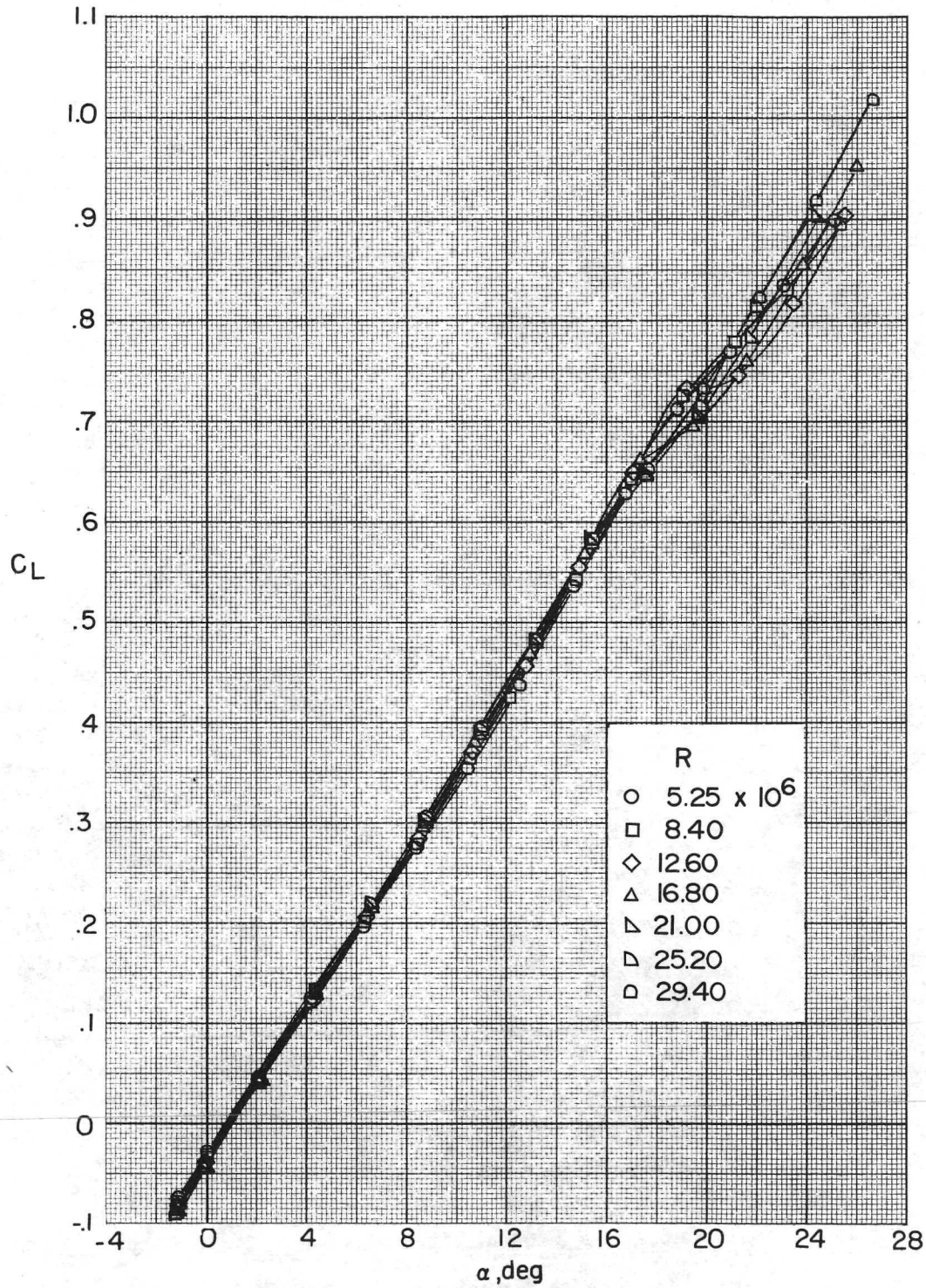

(a) C_L as a function of α.

Figure 4.- Effect of Reynolds number on longitudinal characteristics of model. Natural transition; $\delta_e = 0^o$; BWV_1Z.

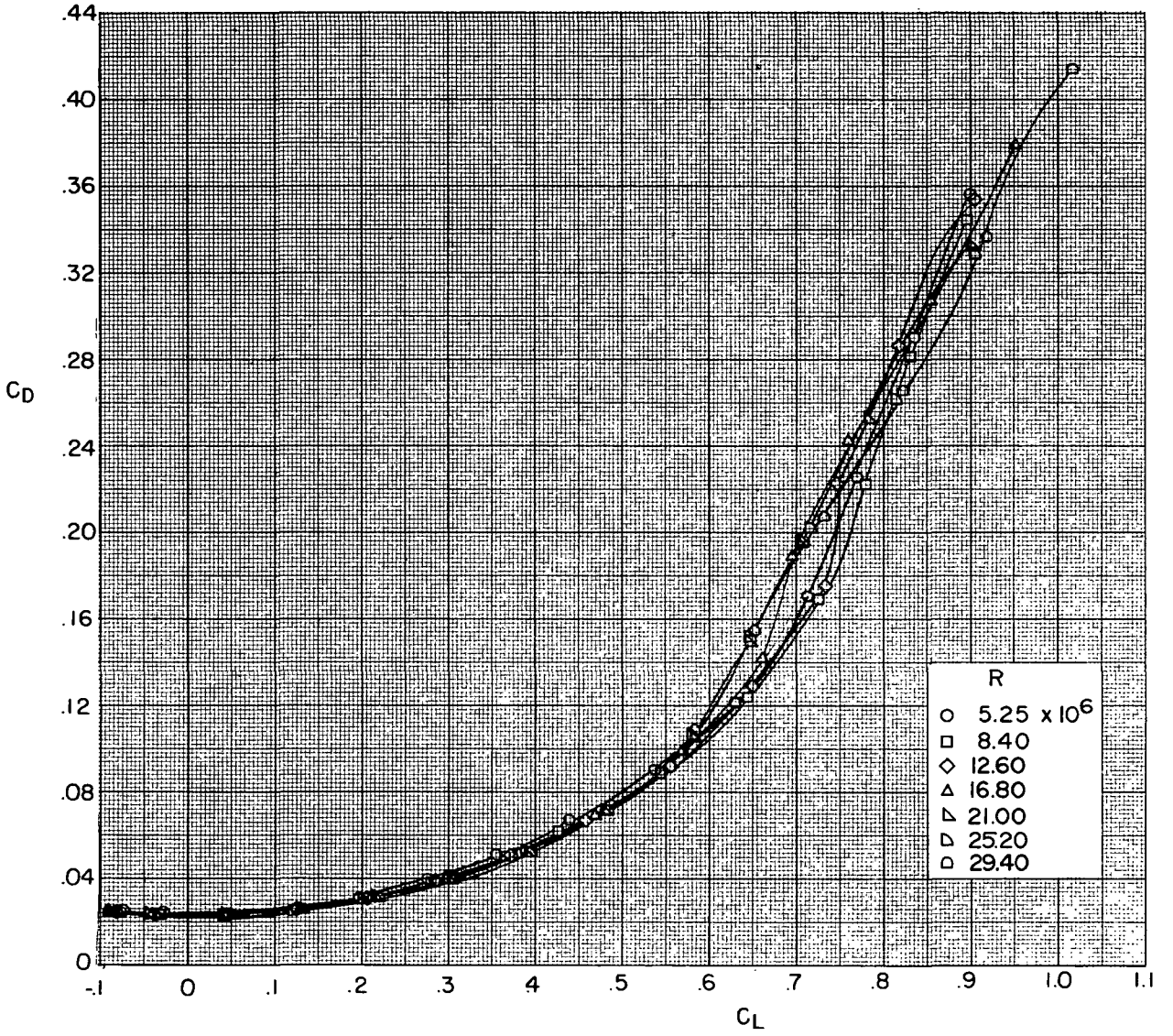

(b) C_D as a function of C_L.

Figure 4.- Continued.

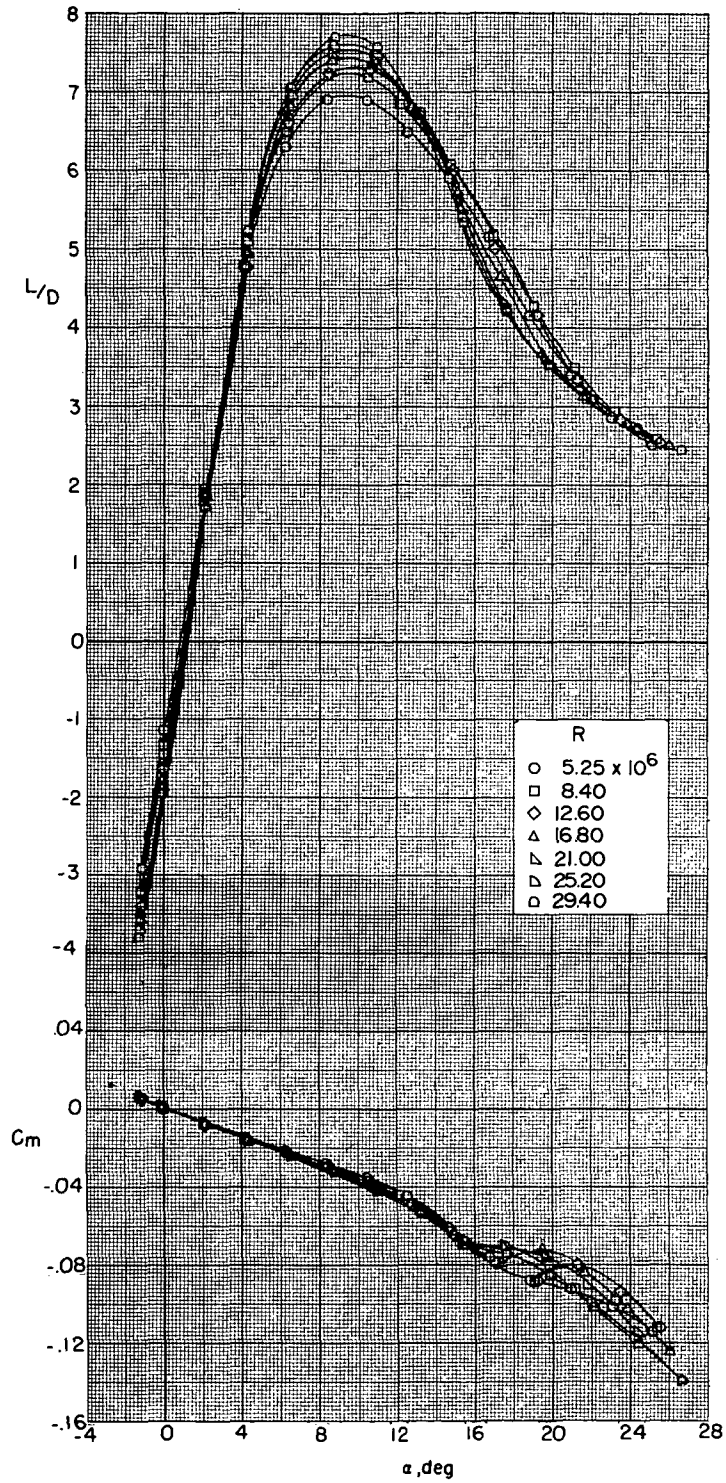

(c) C_m and L/D as a function of α.

Figure 4.- Continued.

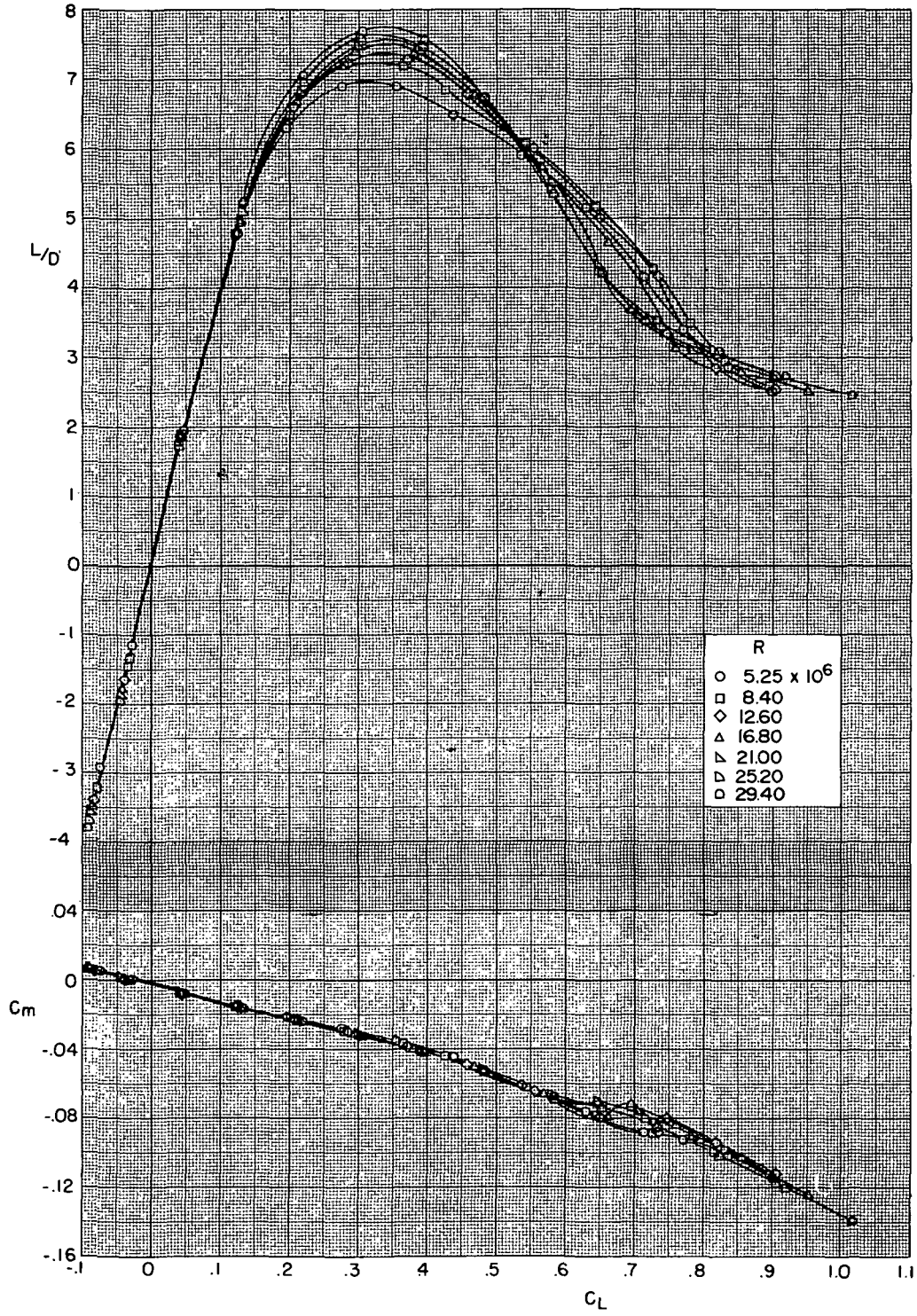

(d) C_m and L/D as a function of C_L.

Figure 4.- Continued.

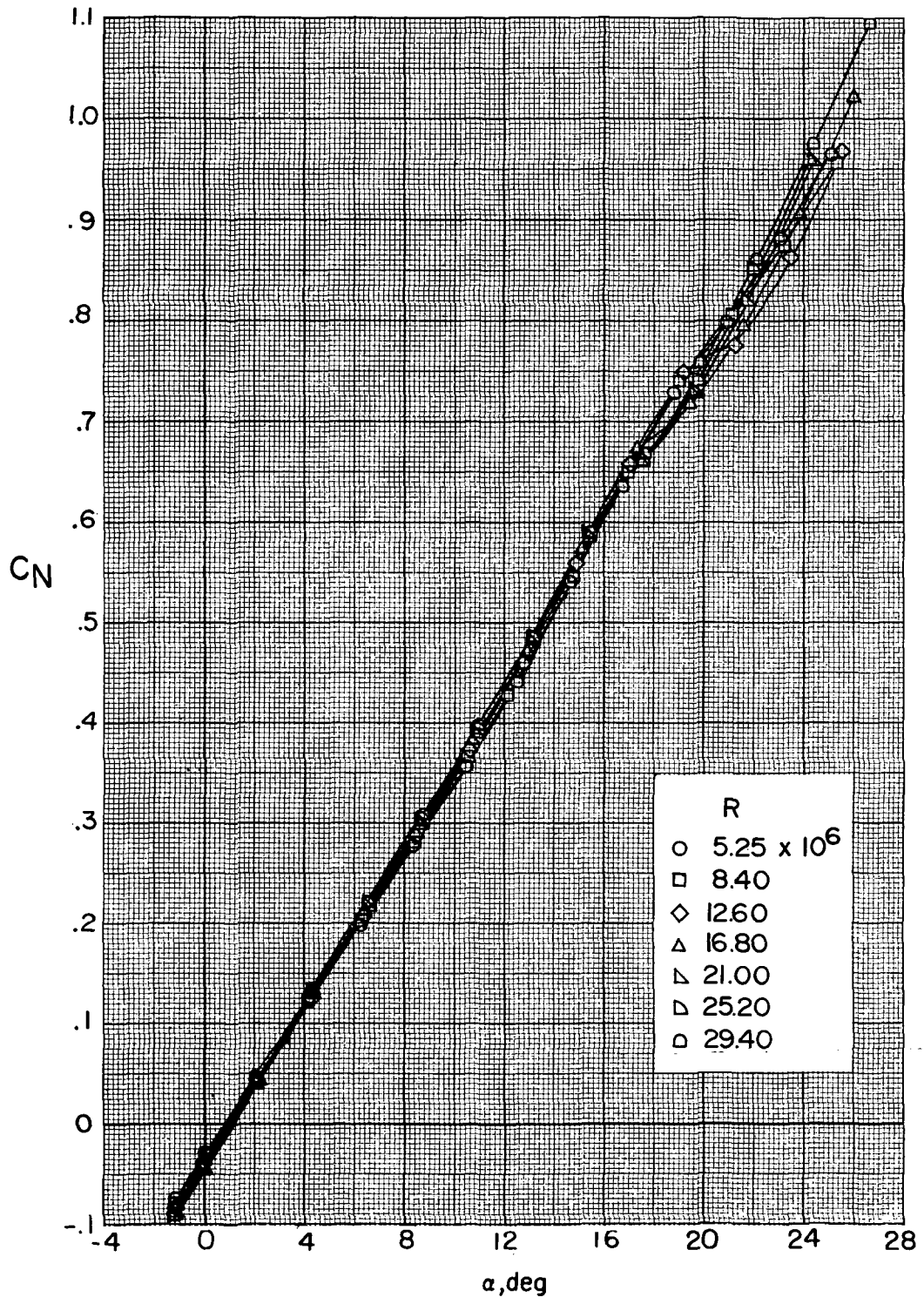

(e) C_N as a function of α.

Figure 4.- Continued.

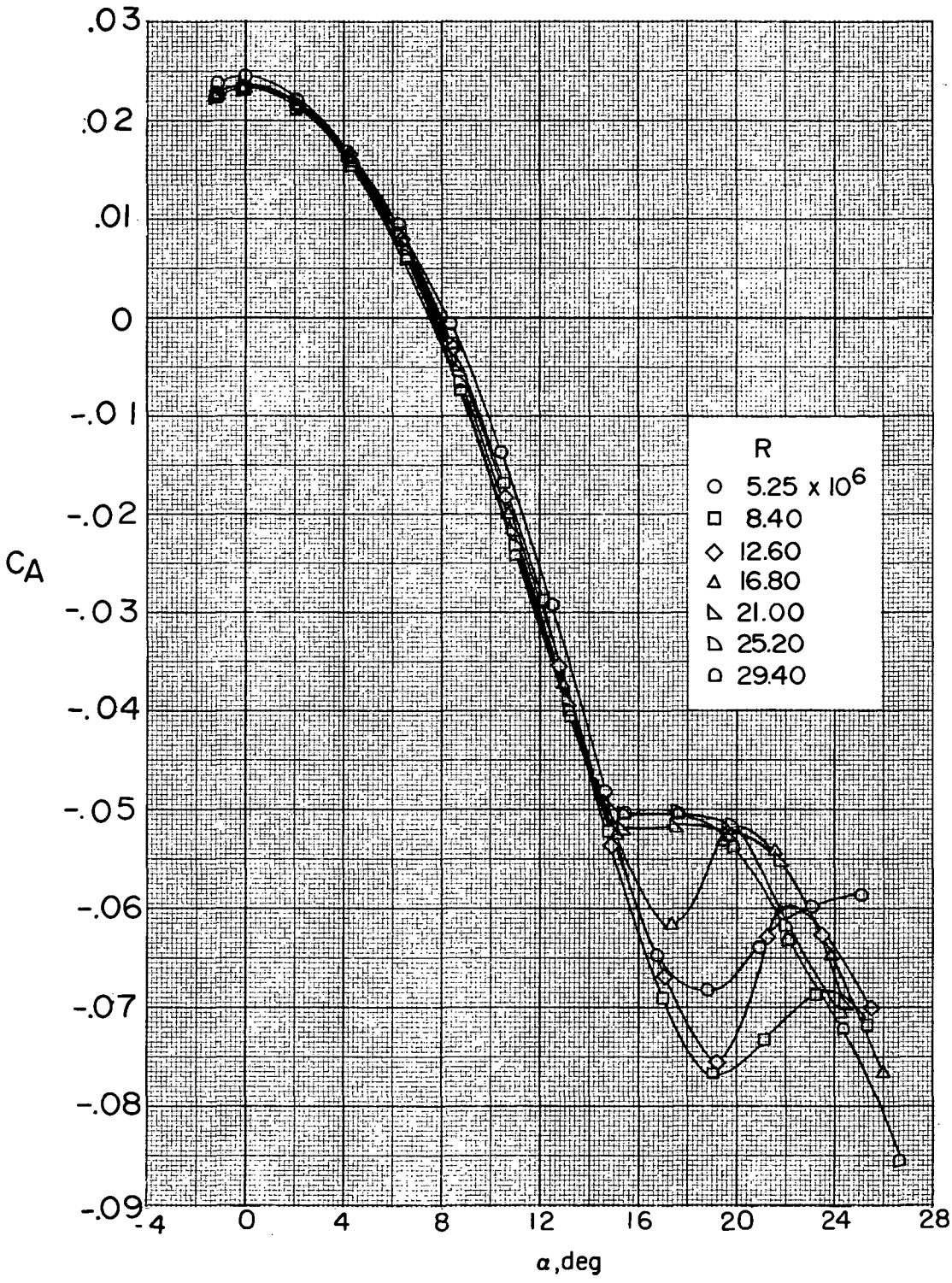

(f) C_A as a function of α.

Figure 4.- Continued.

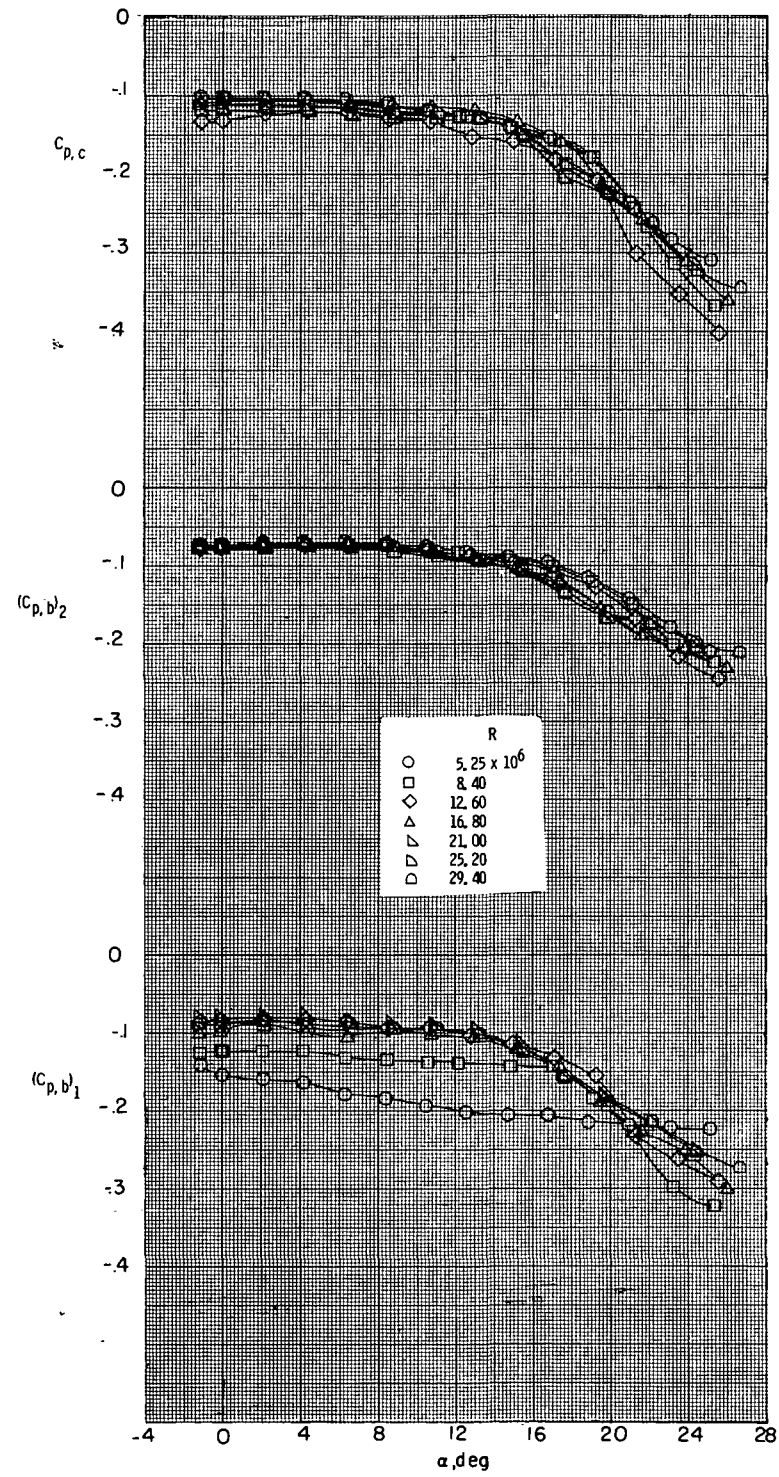

(g) $C_{p,b}$ and $C_{p,c}$ as a function of α.

Figure 4.- Concluded.

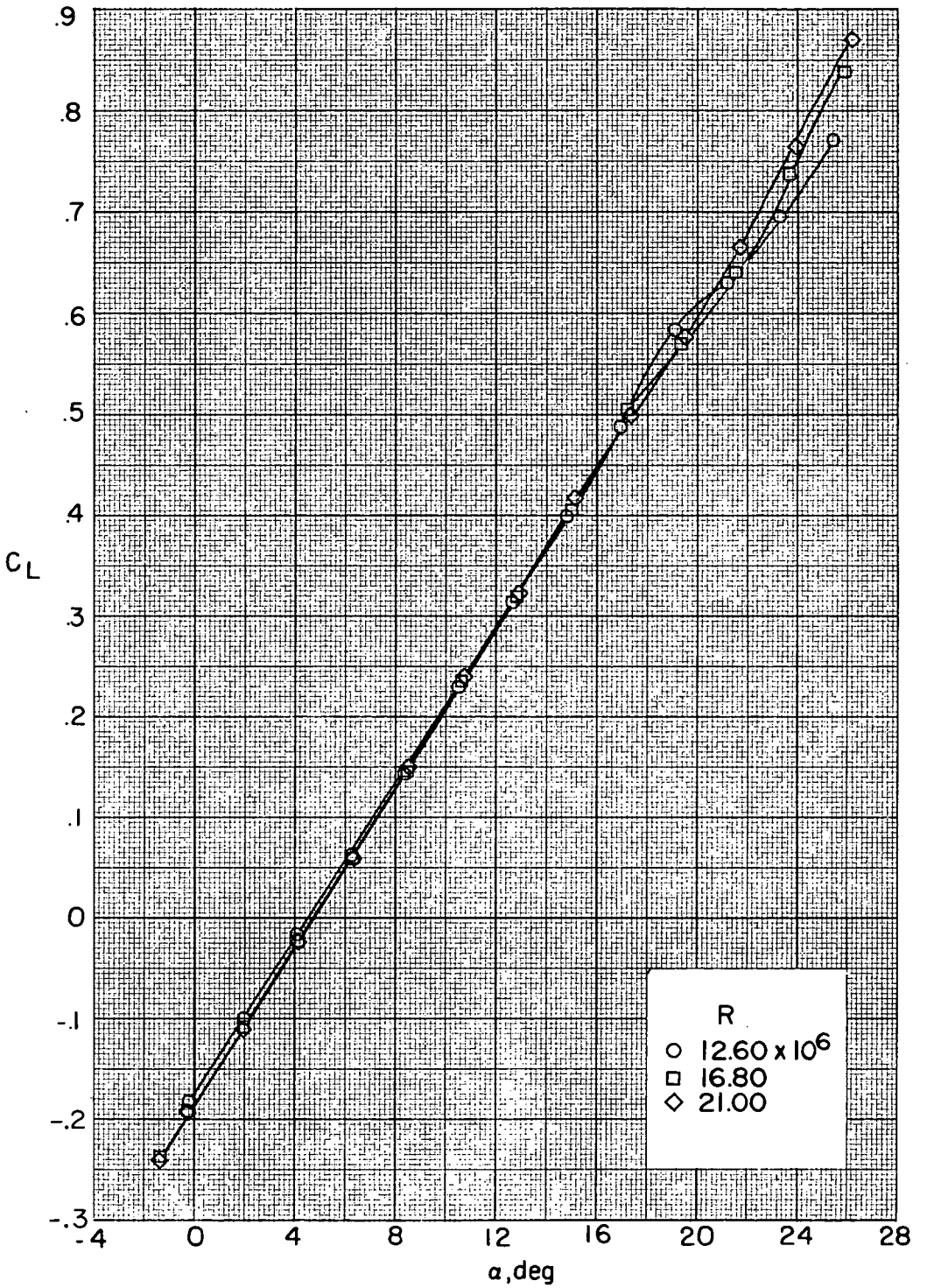

(a) C_L as a function of α.

Figure 5.- Effect of Reynolds number on longitudinal characteristics of model with elevons deflected. Natural transition; $\delta_e = -10.4^o$; BWV_1Z.

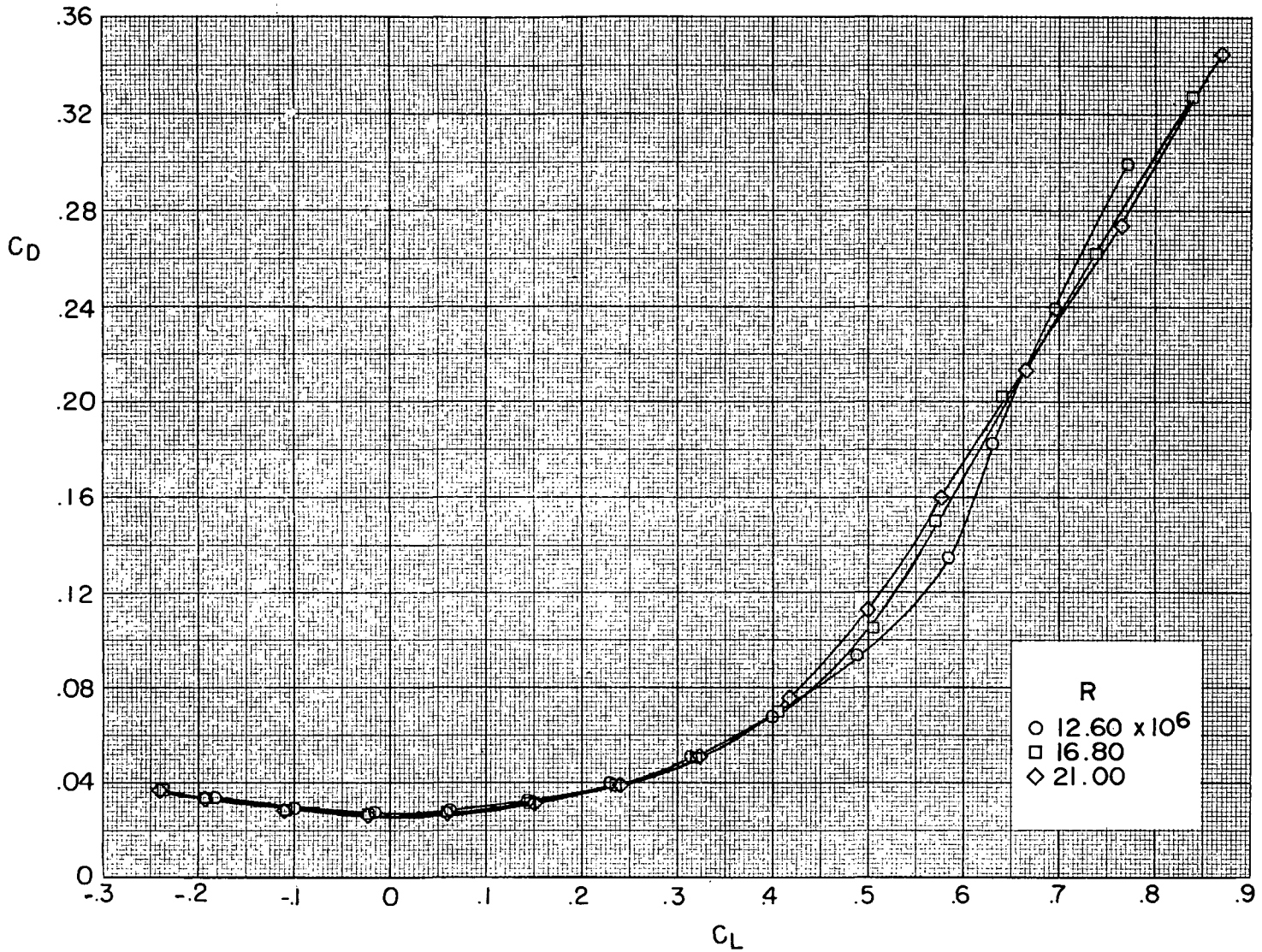

(b) C_D as a function of C_L.

Figure 5.- Continued.

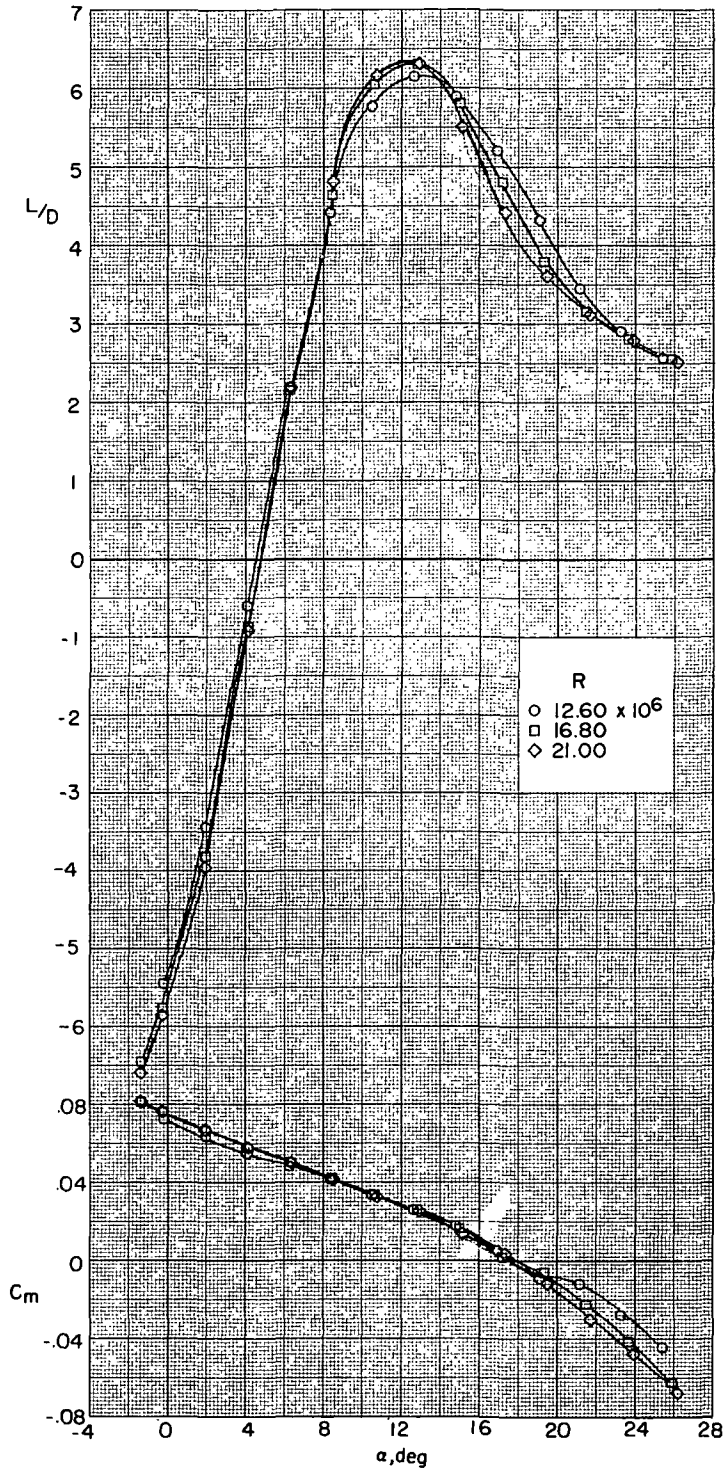

(c) C_m and L/D as a function of α.

Figure 5.- Continued.

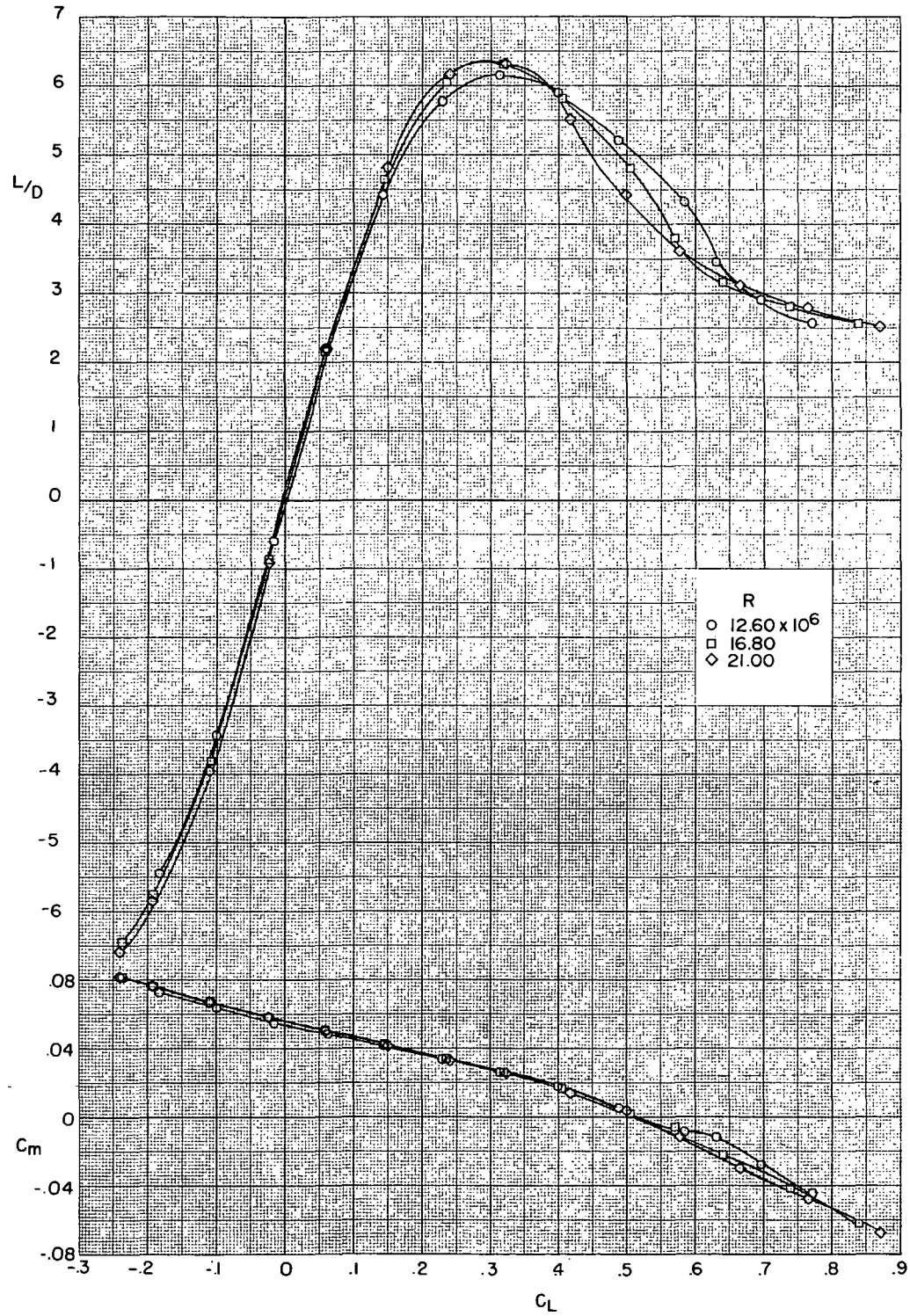

(d) C_m and L/D as a function of C_L.

Figure 5.- Continued.

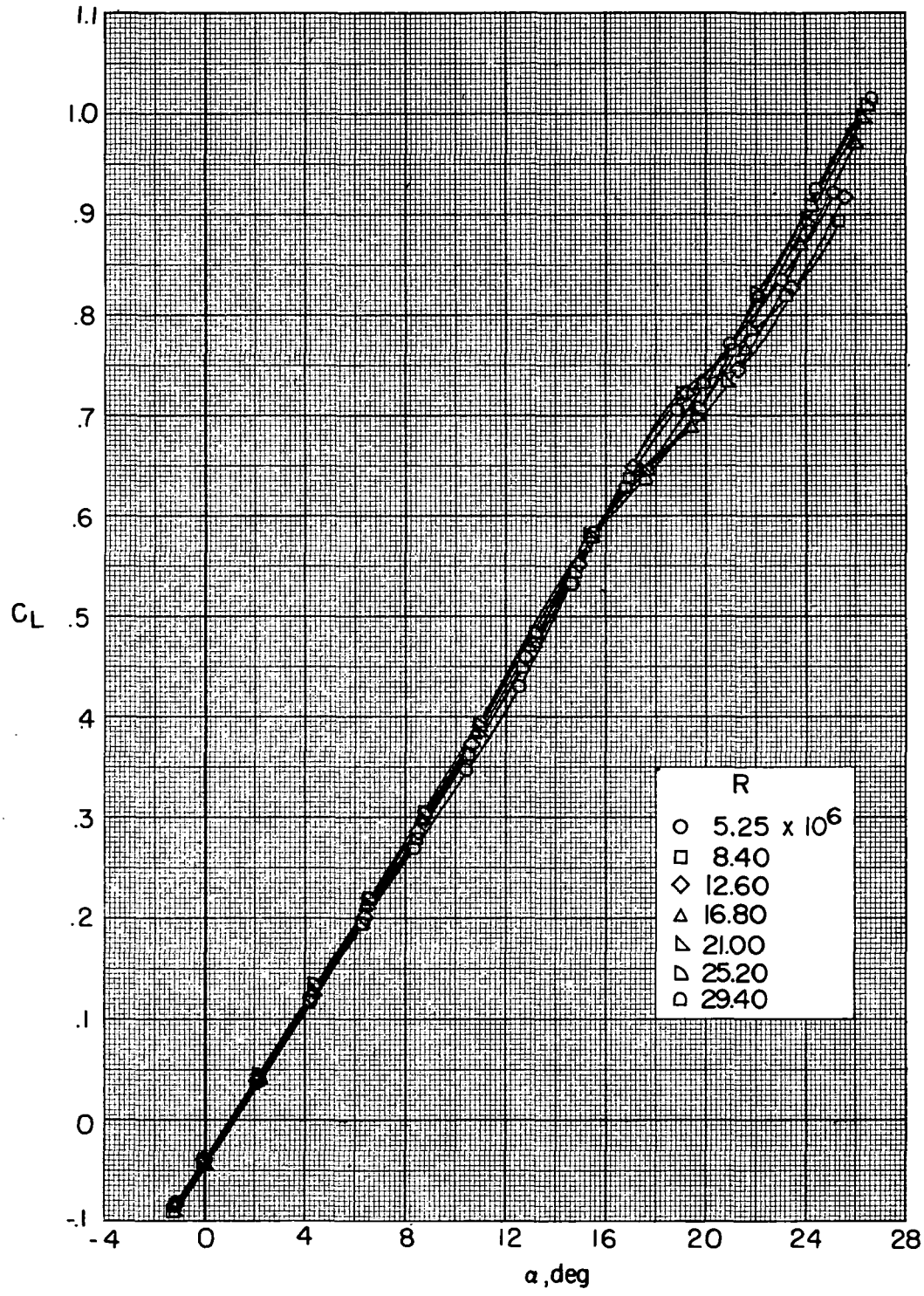

(a) C_L as a function of α.

Figure 6.- Effect of Reynolds number on longitudinal characteristics of model. Fixed transition, 0.0124-cm grit; $\delta_e = 0^o$; BWV_1Z.

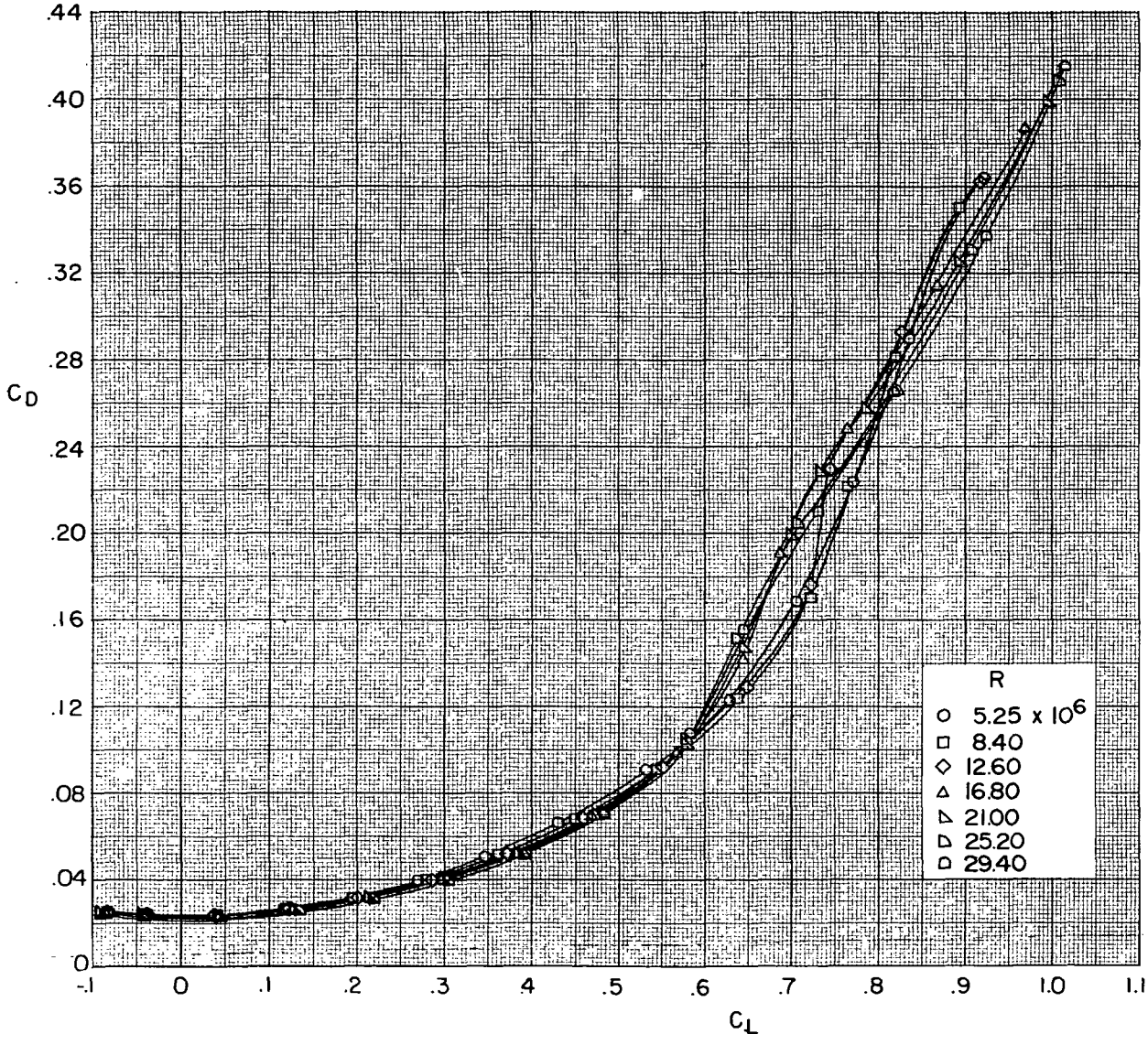

(b) C_D as a function of C_L.

Figure 6.- Continued.

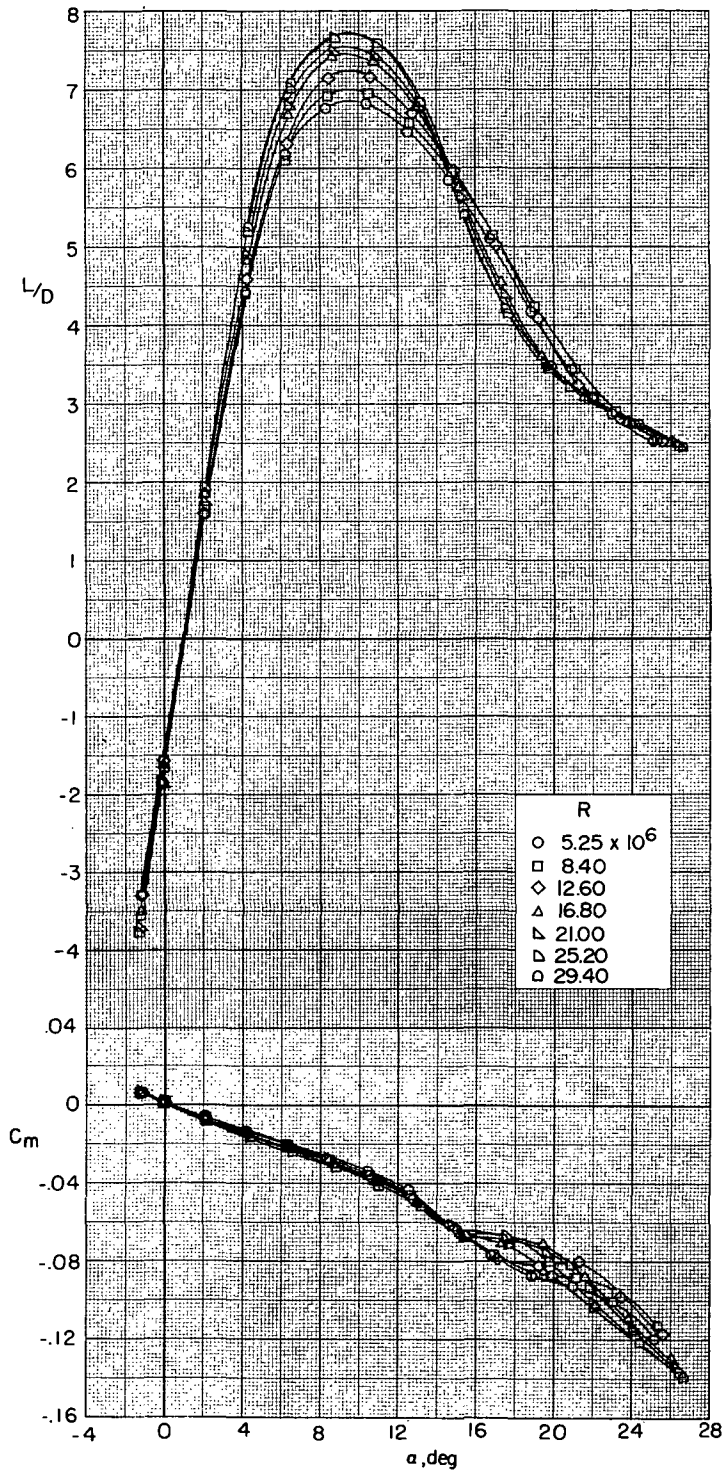

(c) C_m and L/D as a function of α.

Figure 6.- Continued.

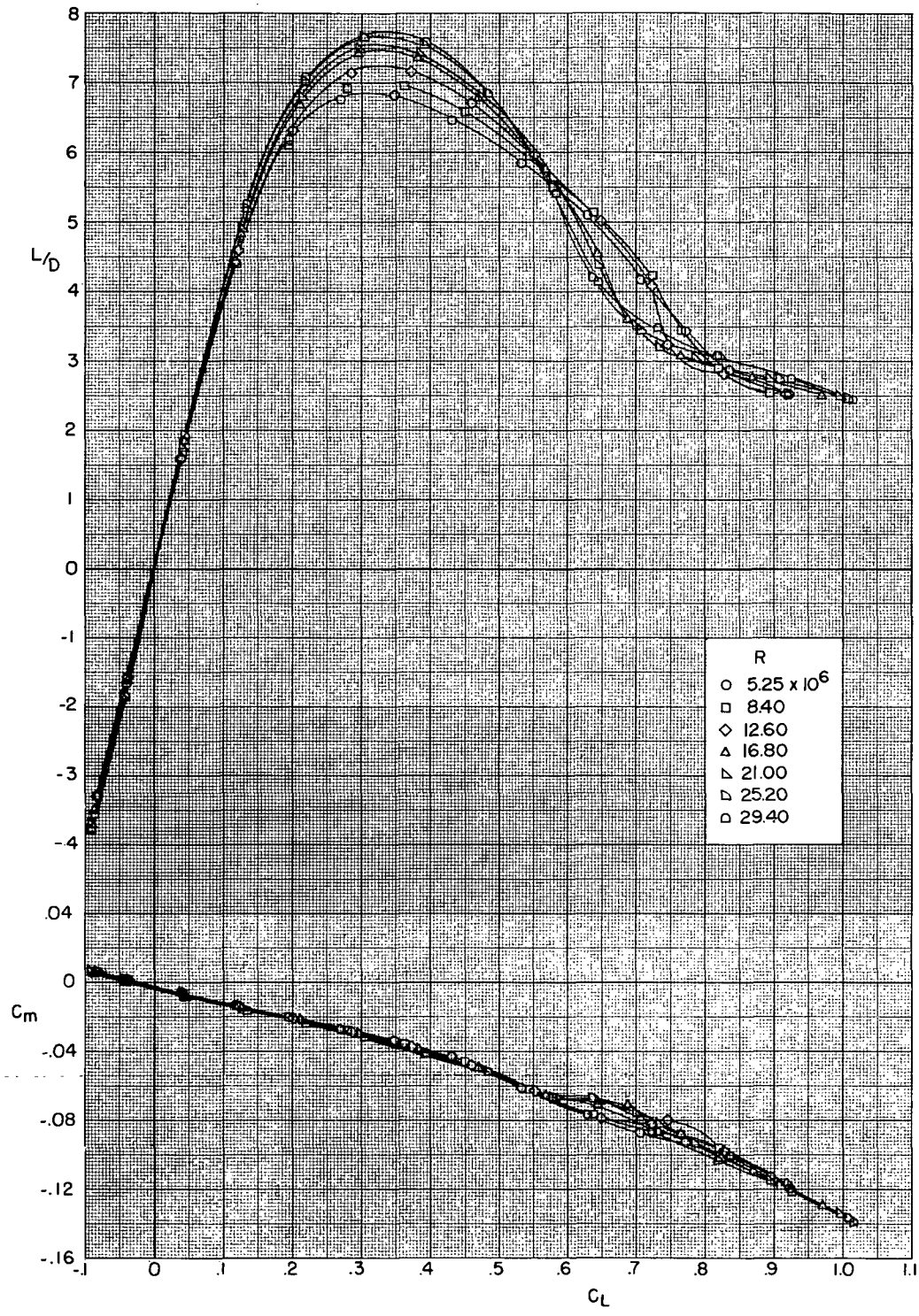

(d) C_m and L/D as a function of C_L.

Figure 6.- Continued.

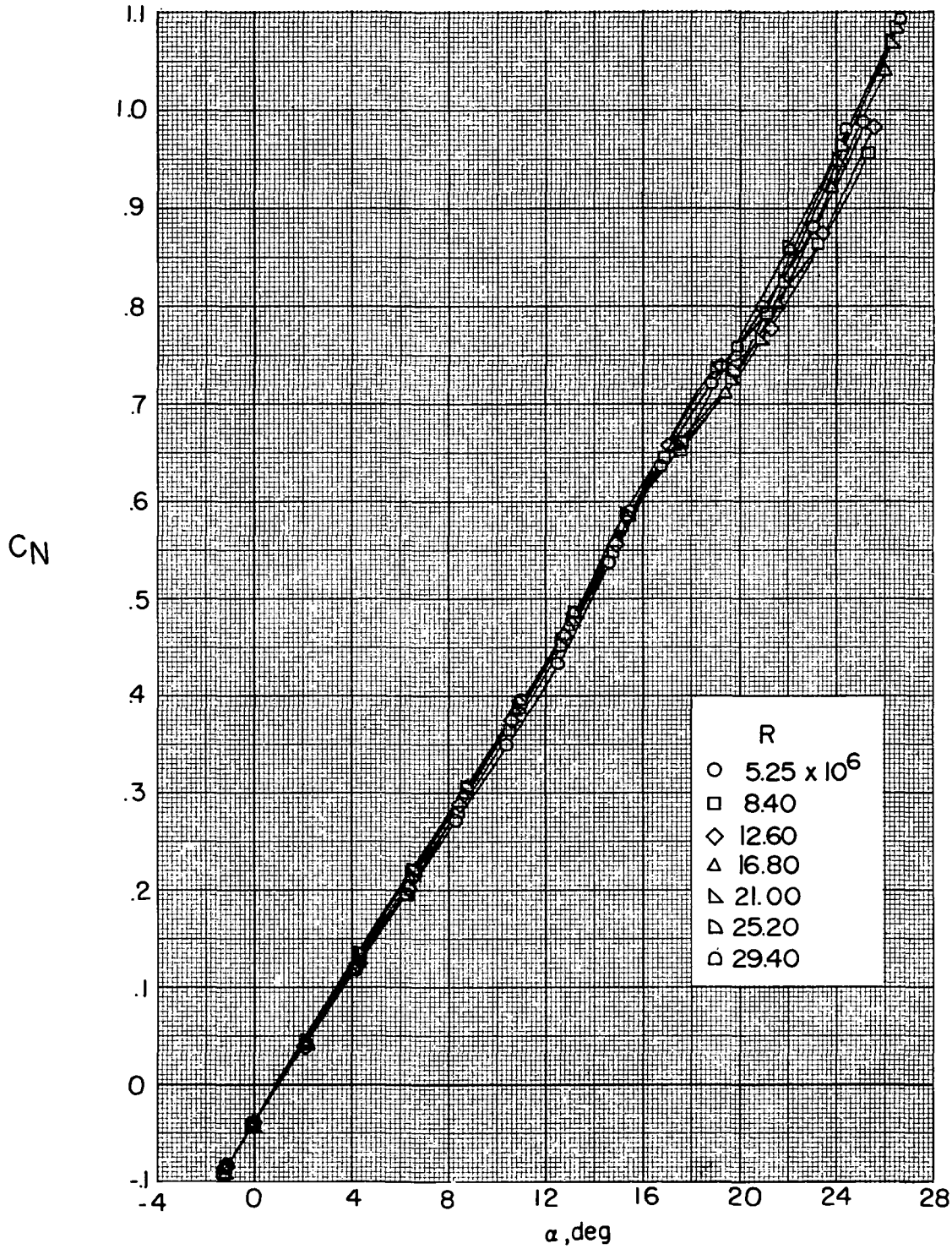

(e) C_N as a function of α.

Figure 6.- Continued.

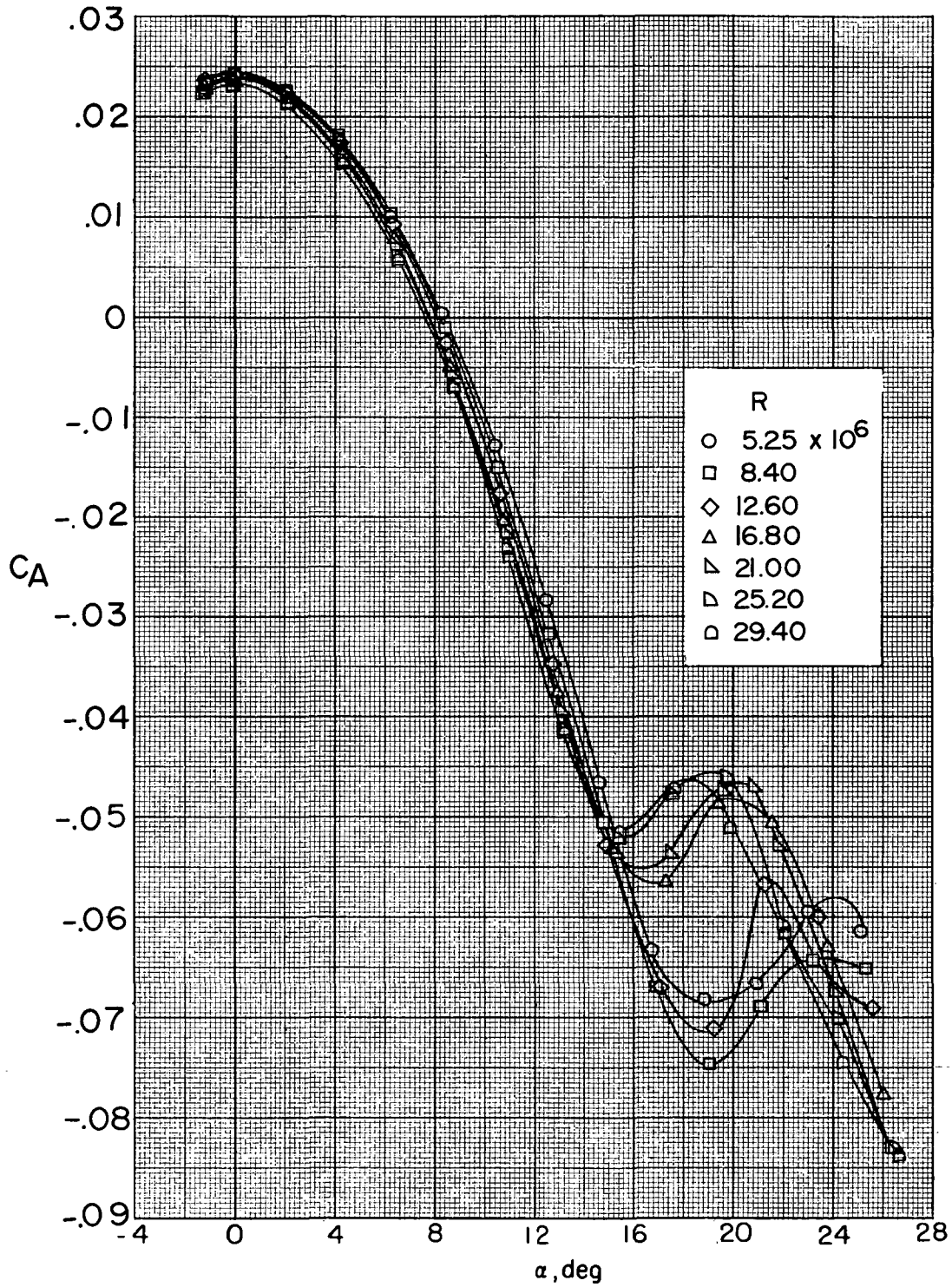

(f) C_A as a function of α.

Figure 6.- Continued.

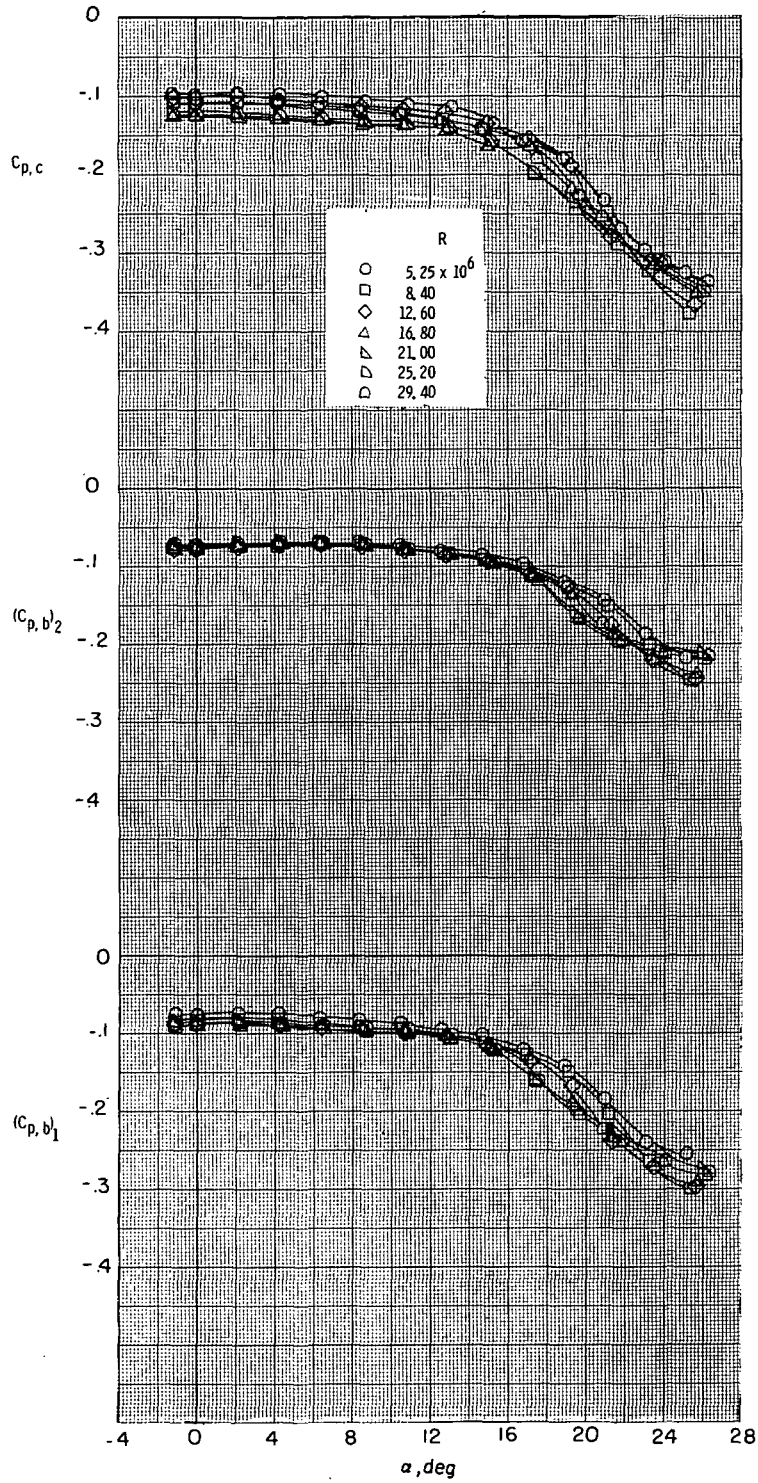

(g) $C_{p,b}$ and $C_{p,c}$ as a function of α.

Figure 6.- Concluded.

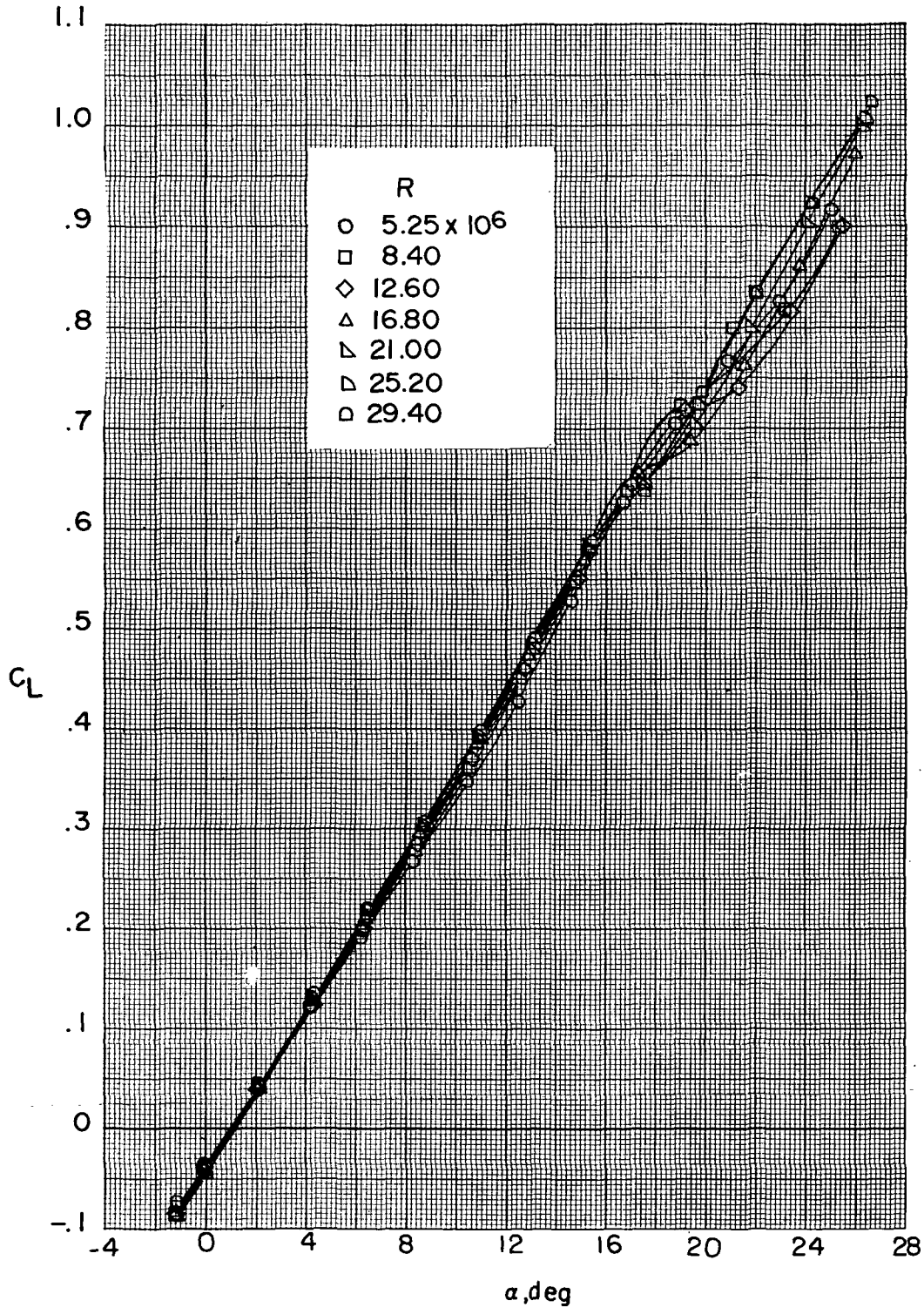

(a) C_L as a function of α.

Figure 7.- Effect of Reynolds number on longitudinal characteristics of model. Fixed transition, 0.0073-cm grit; $\delta_e = 0^o$; BWV_1Z.

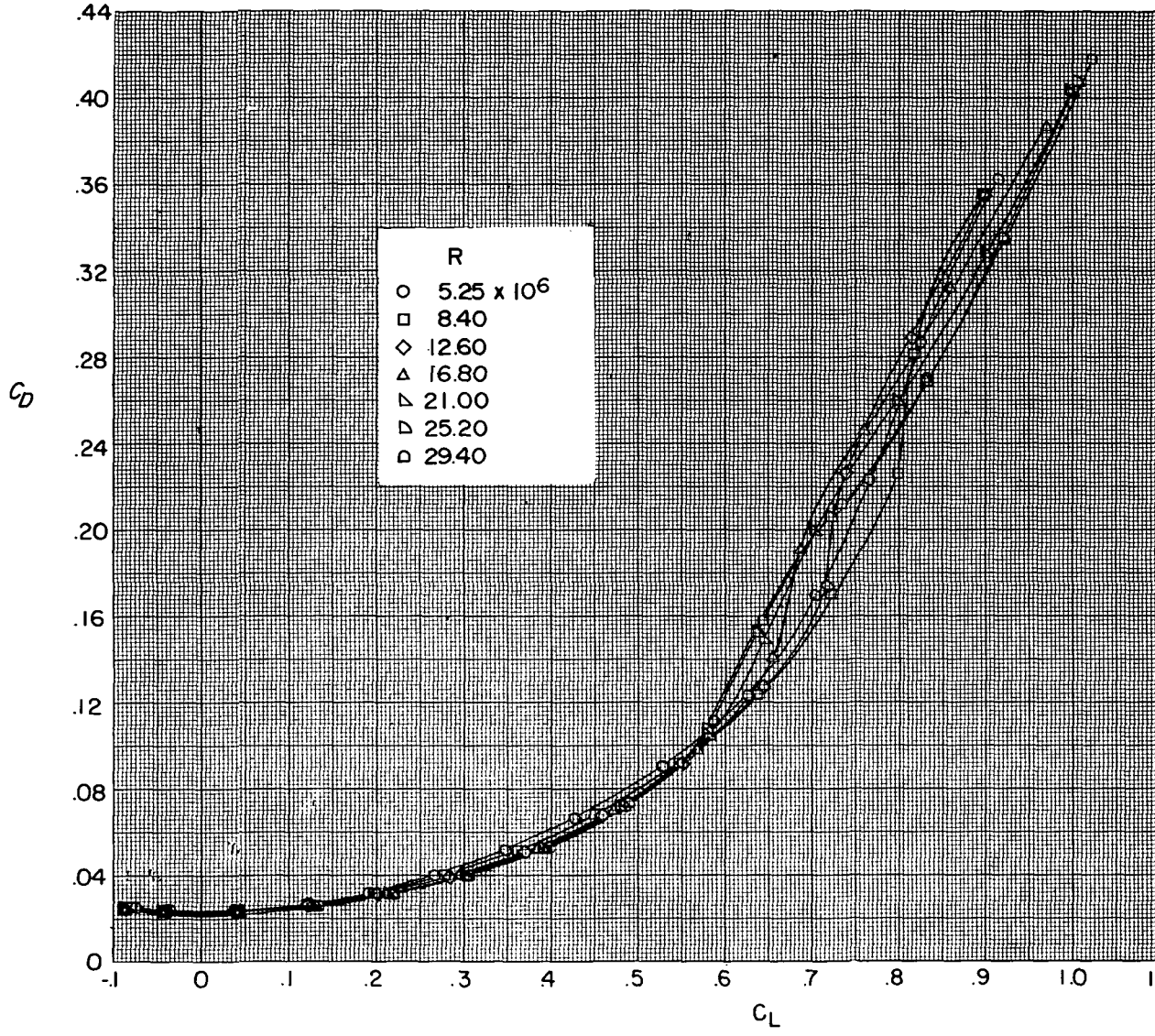

(b) C_D as a function of C_L.

Figure 7.- Continued.

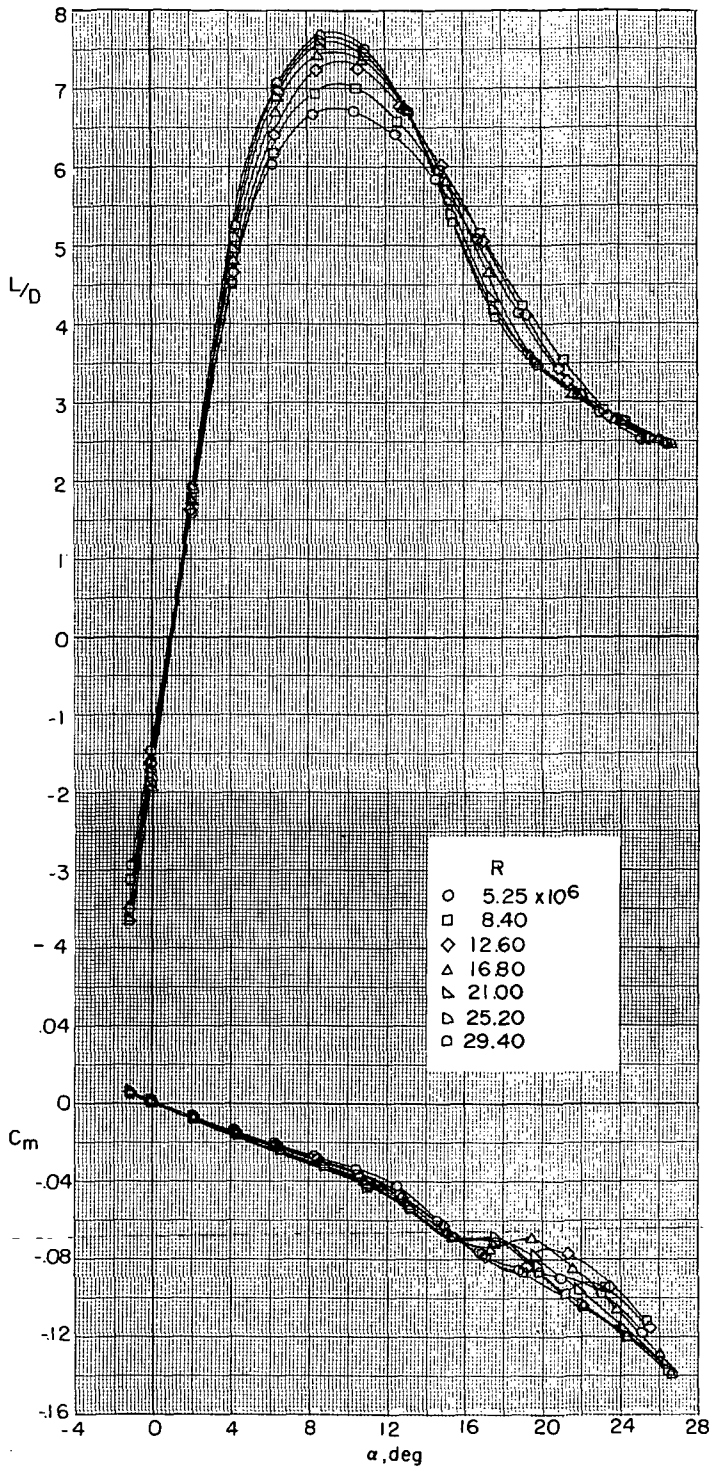

(c) C_m and L/D as a function of α.

Figure 7.- Continued.

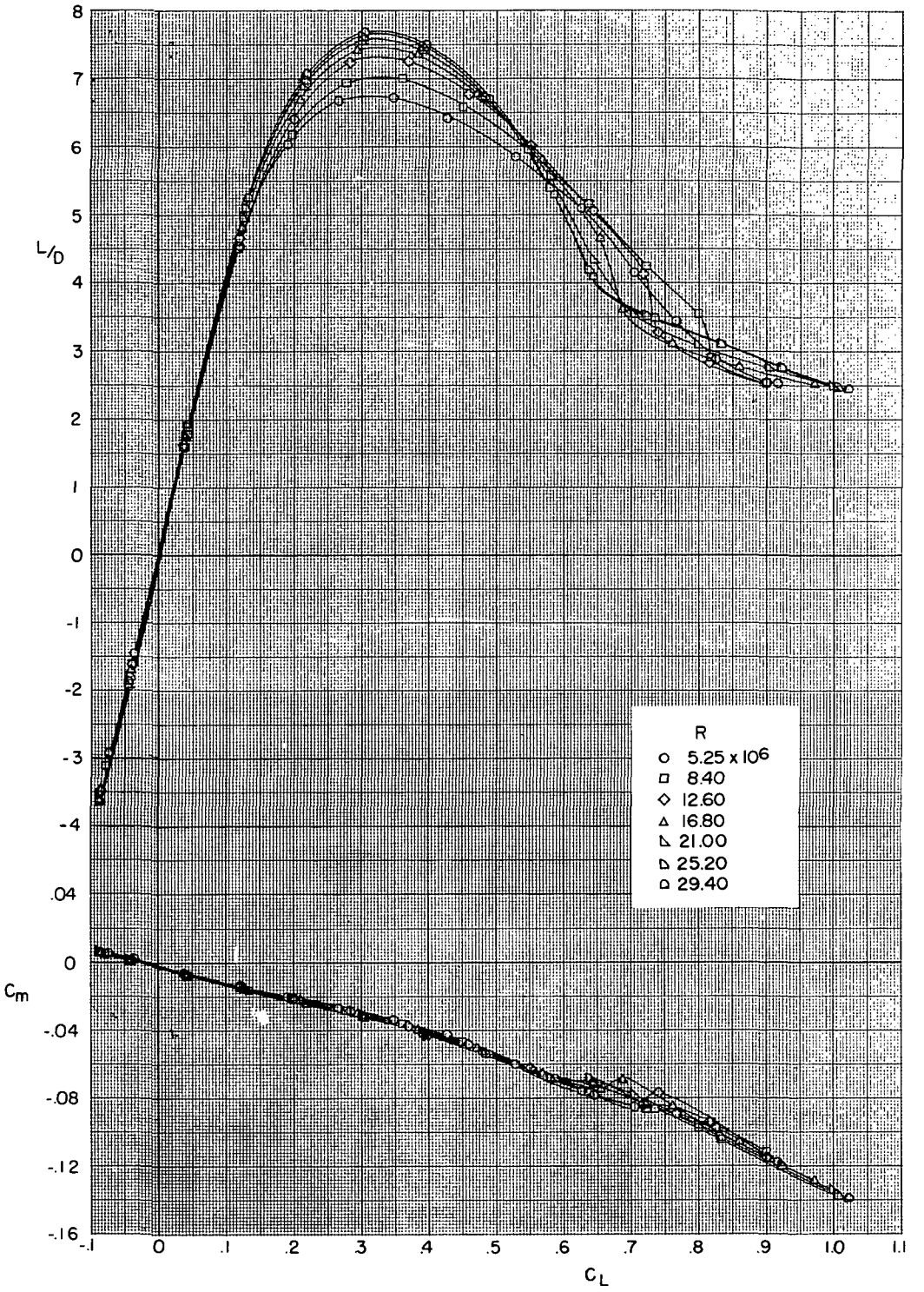

(d) C_m and L/D as a function of C_L.

Figure 7.- Continued.

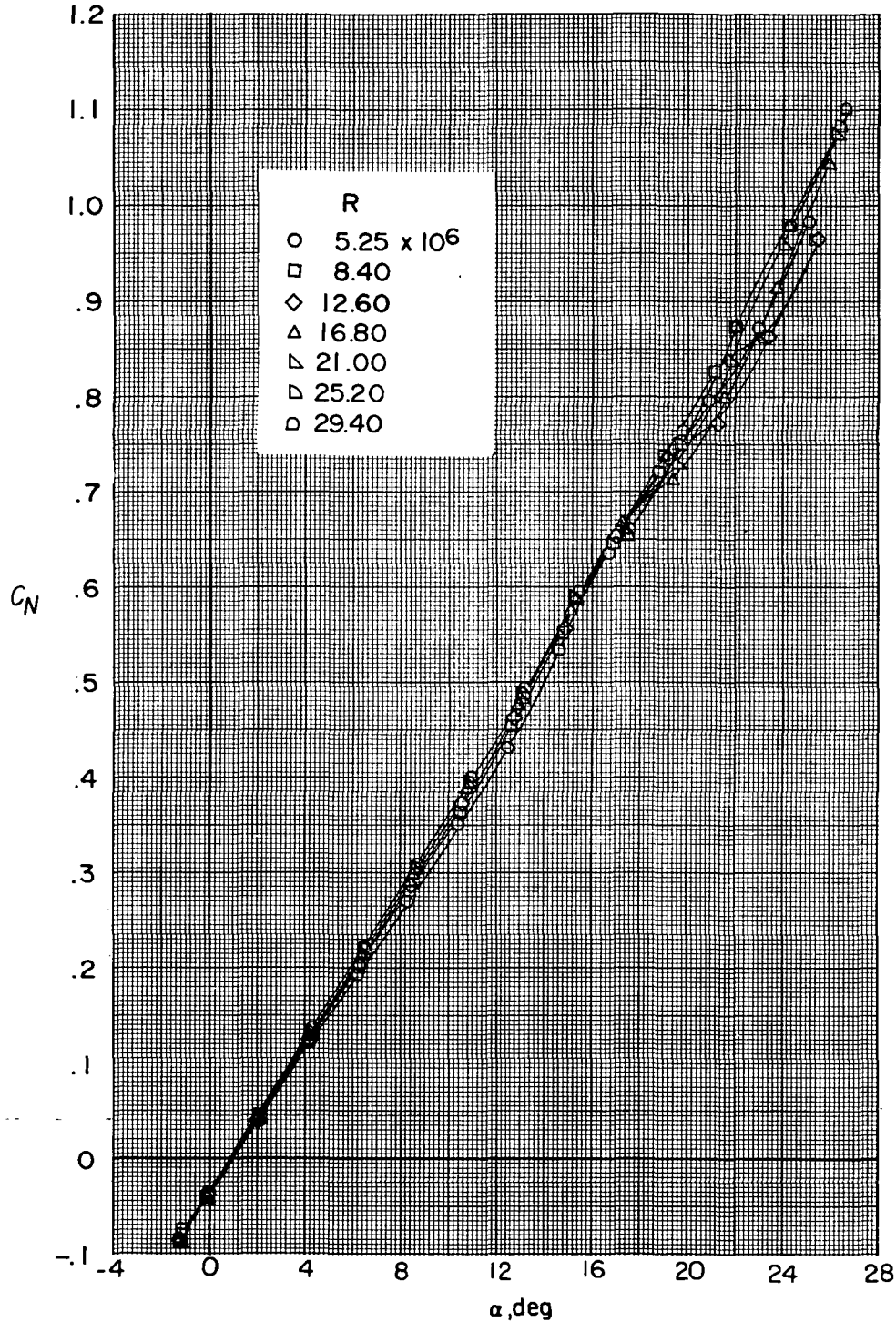

(e) C_N as a function of α.

Figure 7.- Continued.

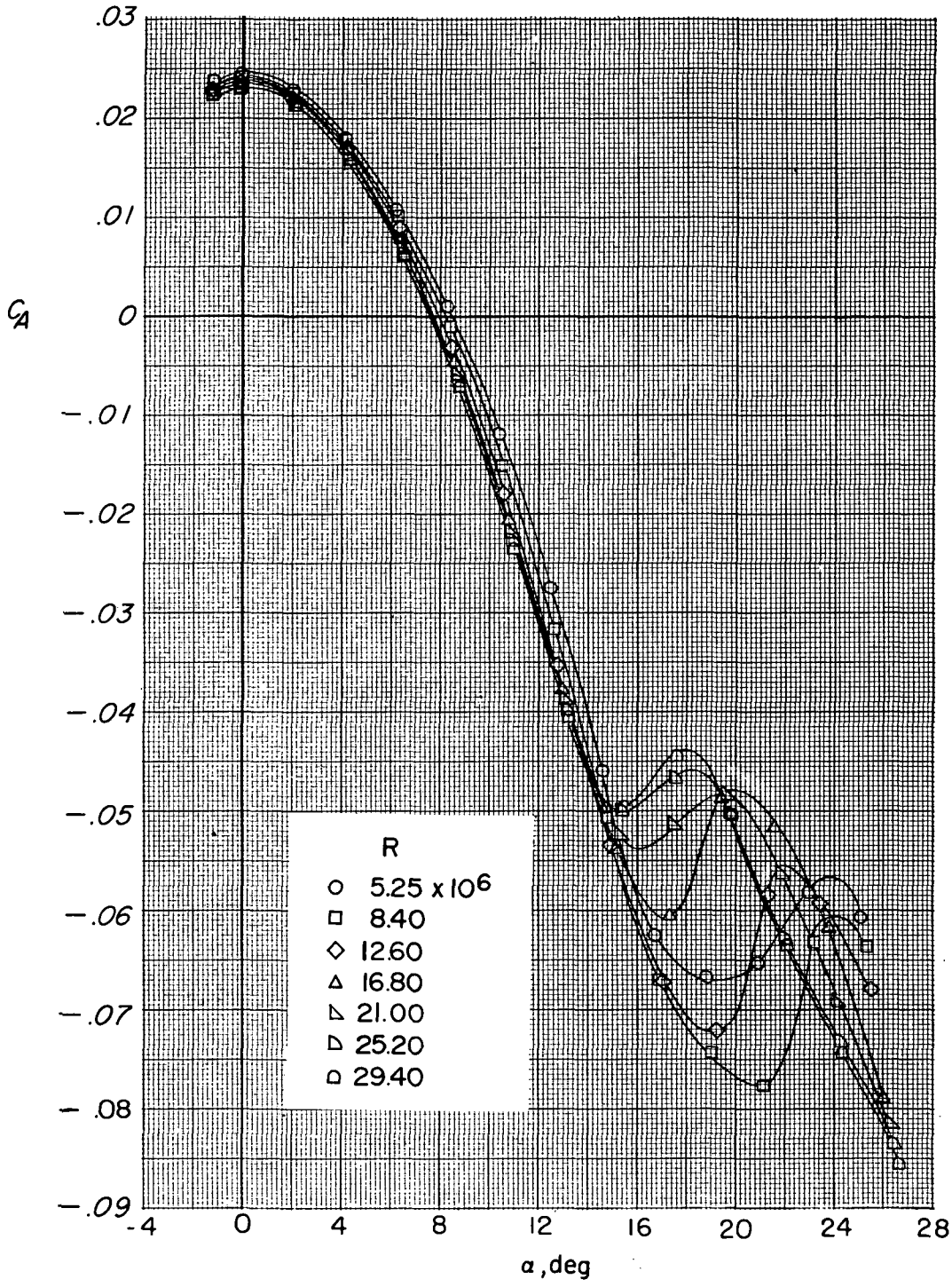

(f) C_A as a function of α.

Figure 7.- Continued.

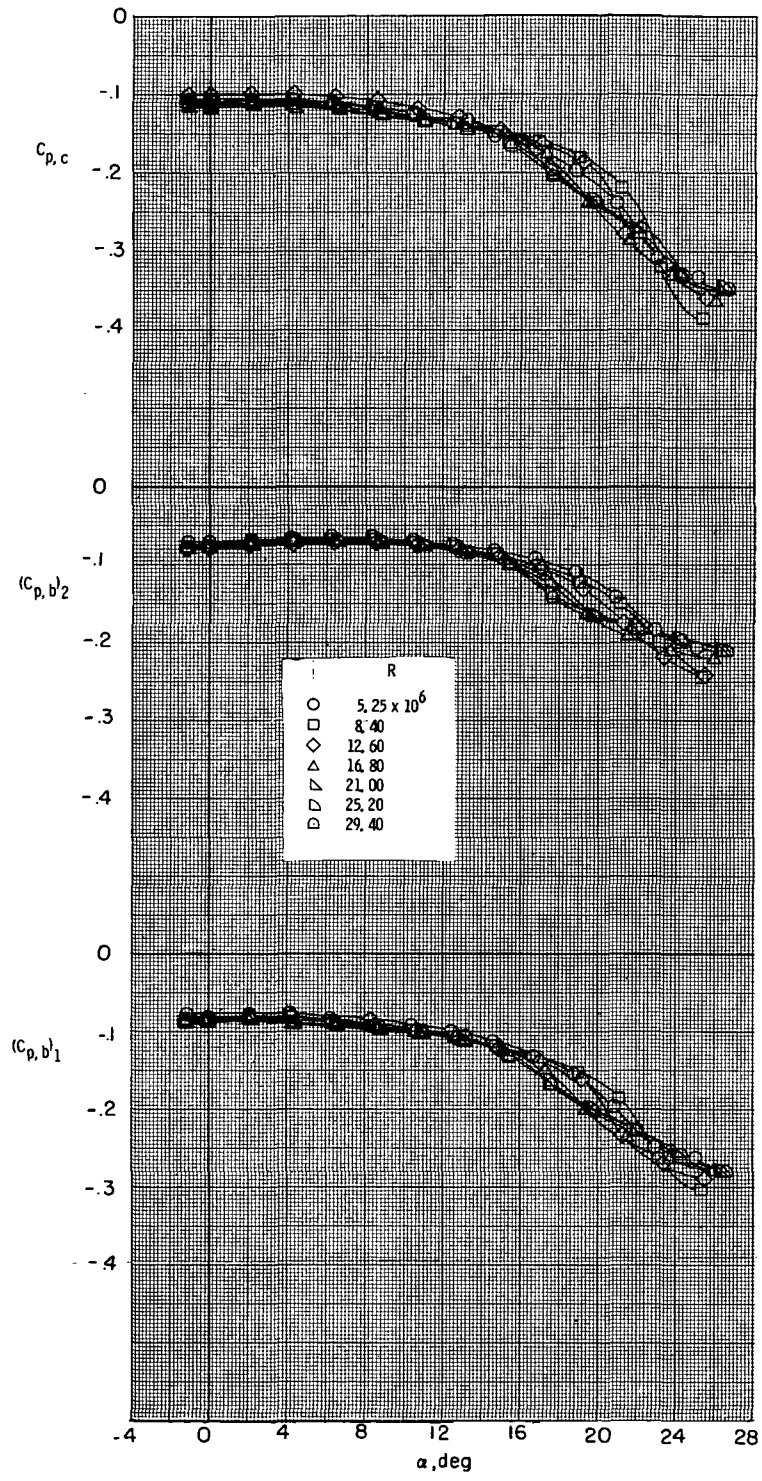

(g) $C_{p,b}$ and $C_{p,c}$ as a function of α.

Figure 7.- Concluded.

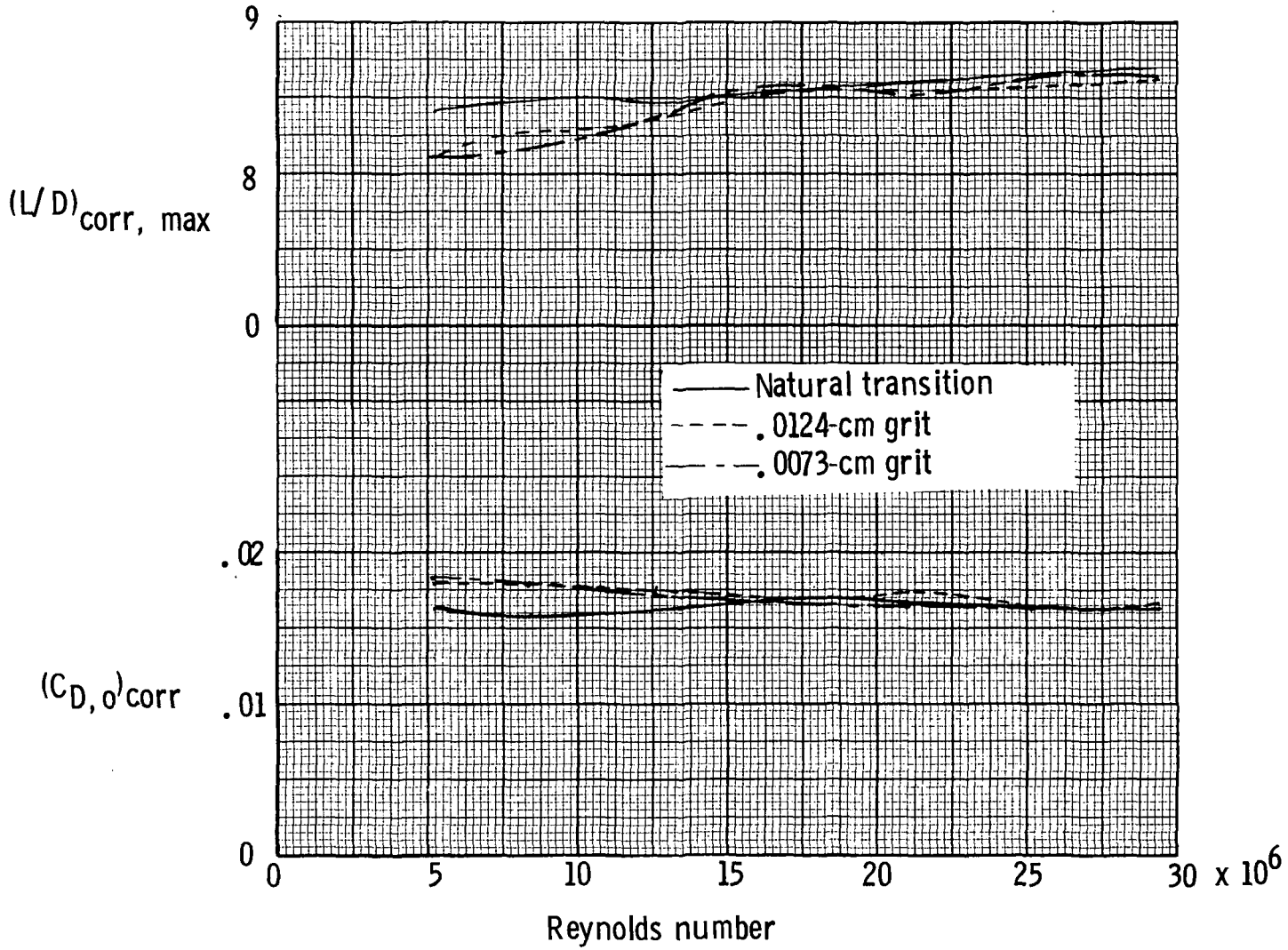

Figure 8.- Effect of Reynolds number and fixed transition on $(L/D)_{corr,max}$ and $(C_{D,o})_{corr}$.

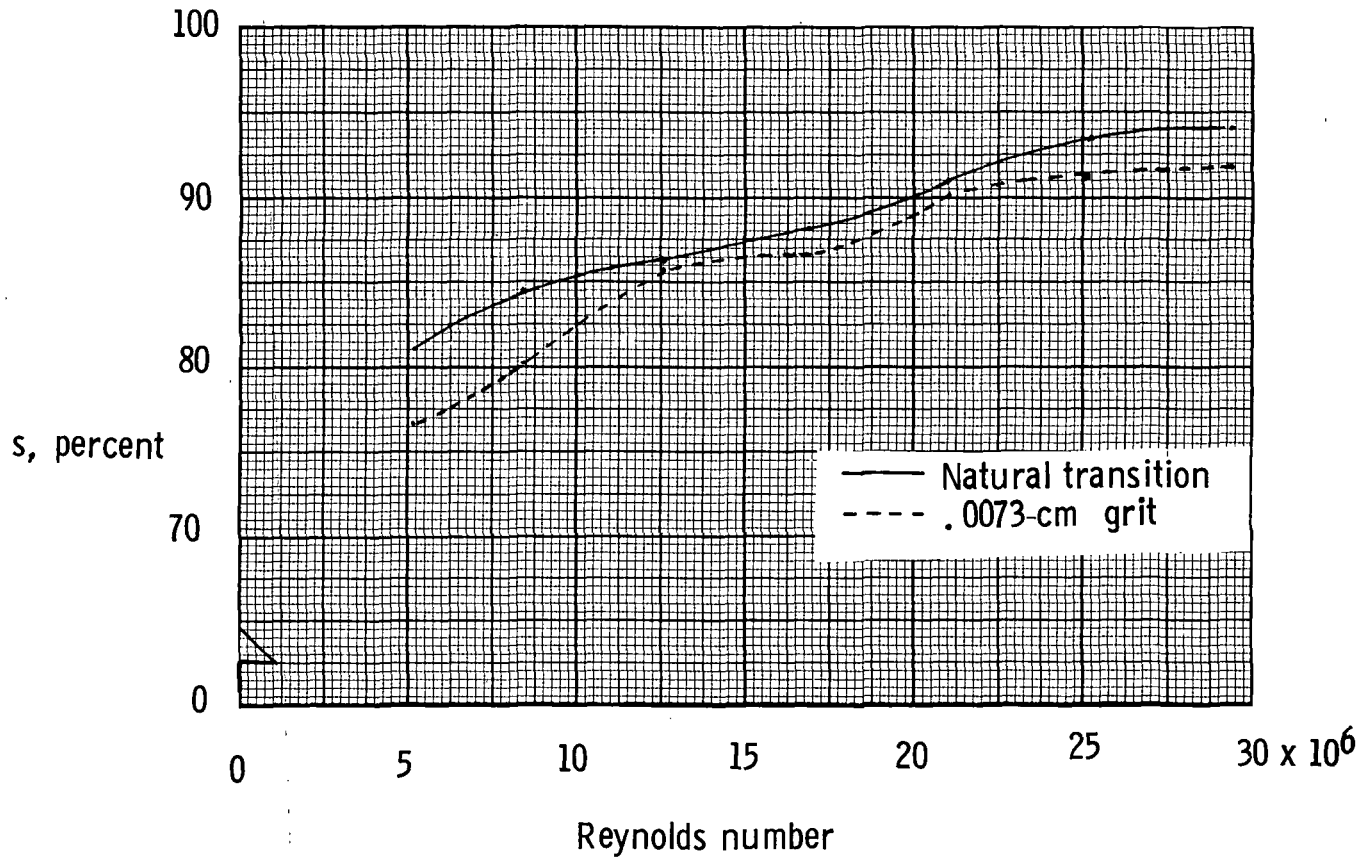

Figure 9.- Effect of Reynolds number on leading-edge suction parameter for model.

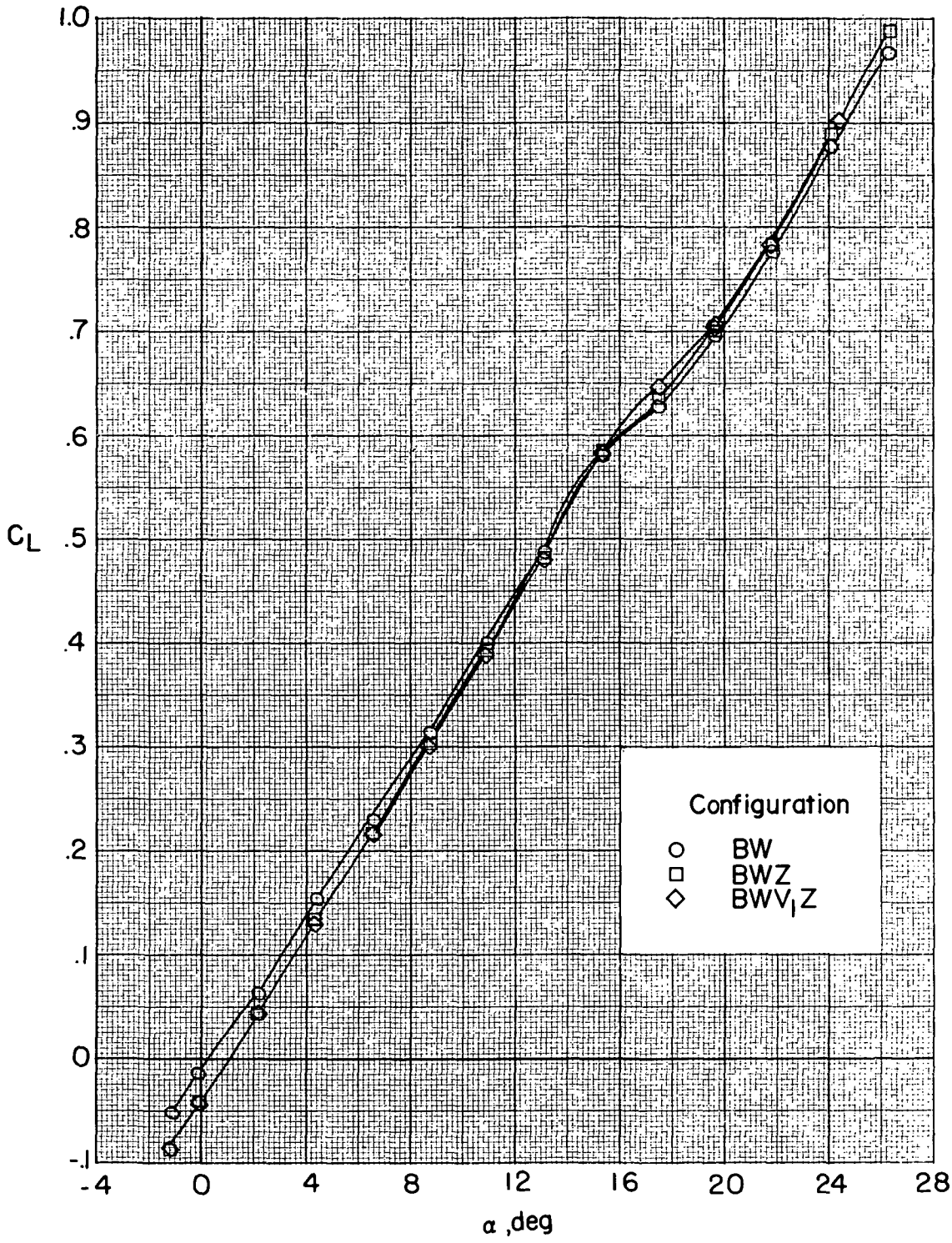

(a) C_L as a function of α.

Figure 10.- Configuration buildup. $R = 21.0 \times 10^6$; $\delta_e = 0^o$.

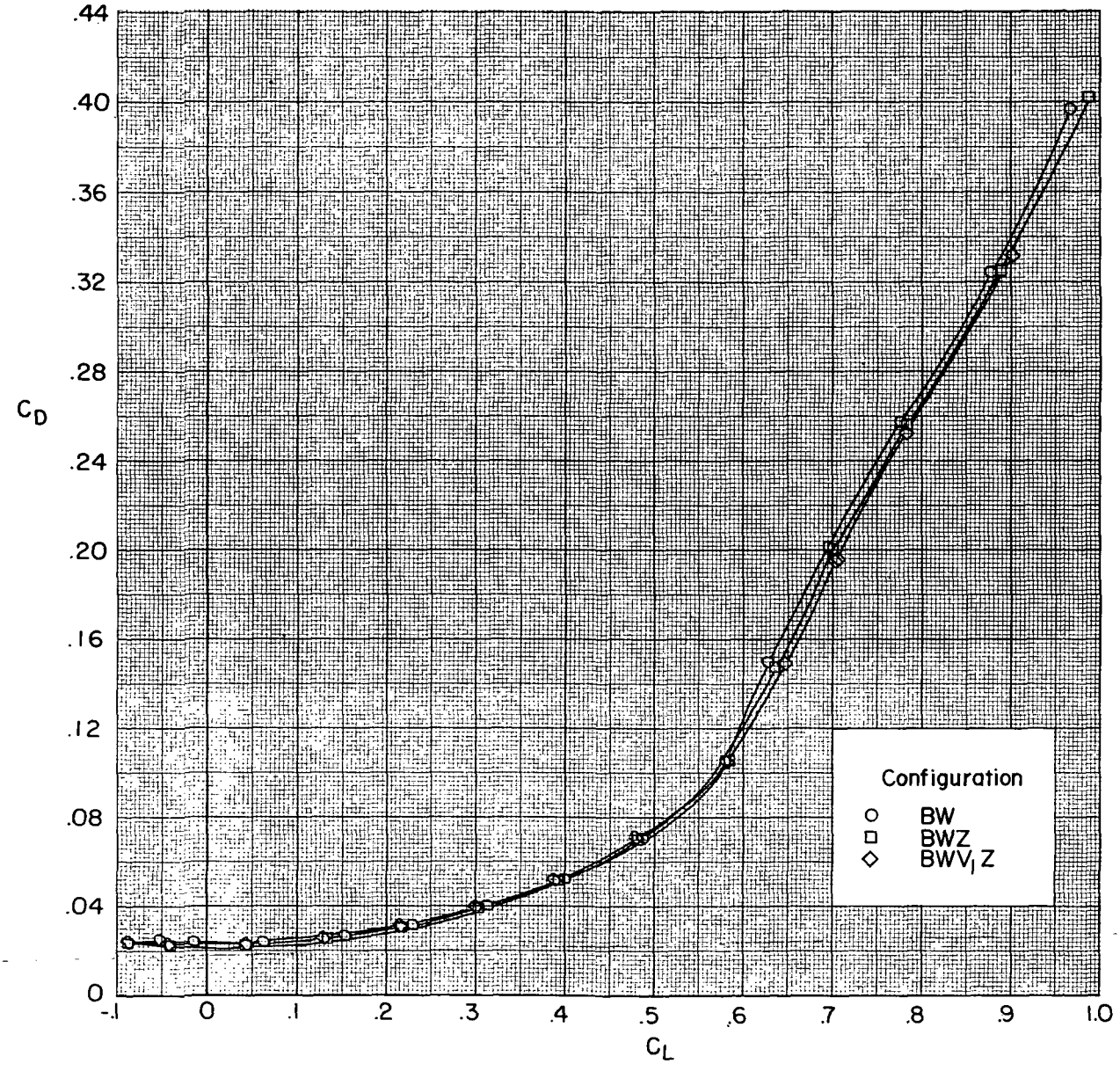

(b) C_D as a function of C_L.

Figure 10.- Continued.

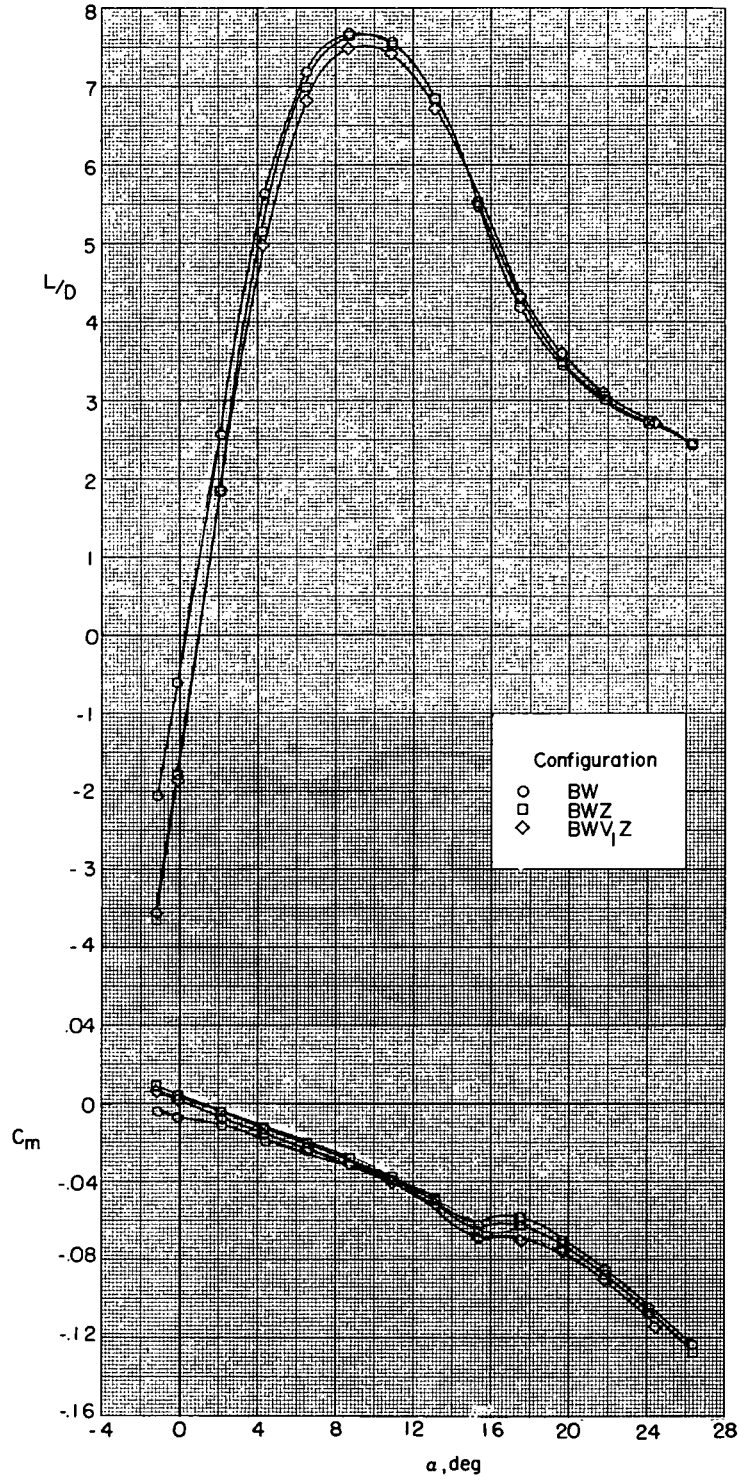

(c) C_m and L/D as a function of α.

Figure 10.- Continued.

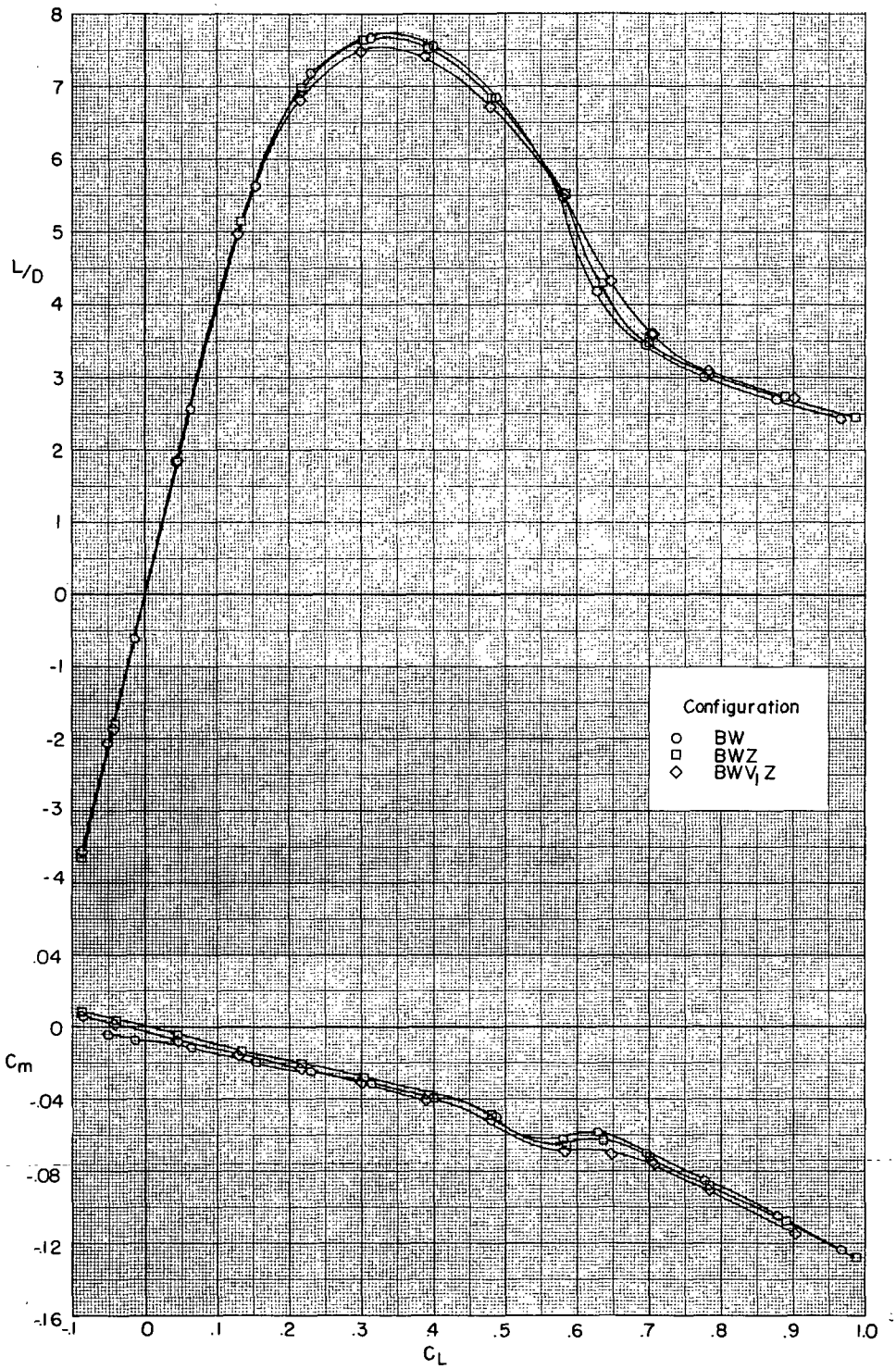

(d) C_m and L/D as a function of C_L.

Figure 10.- Continued.

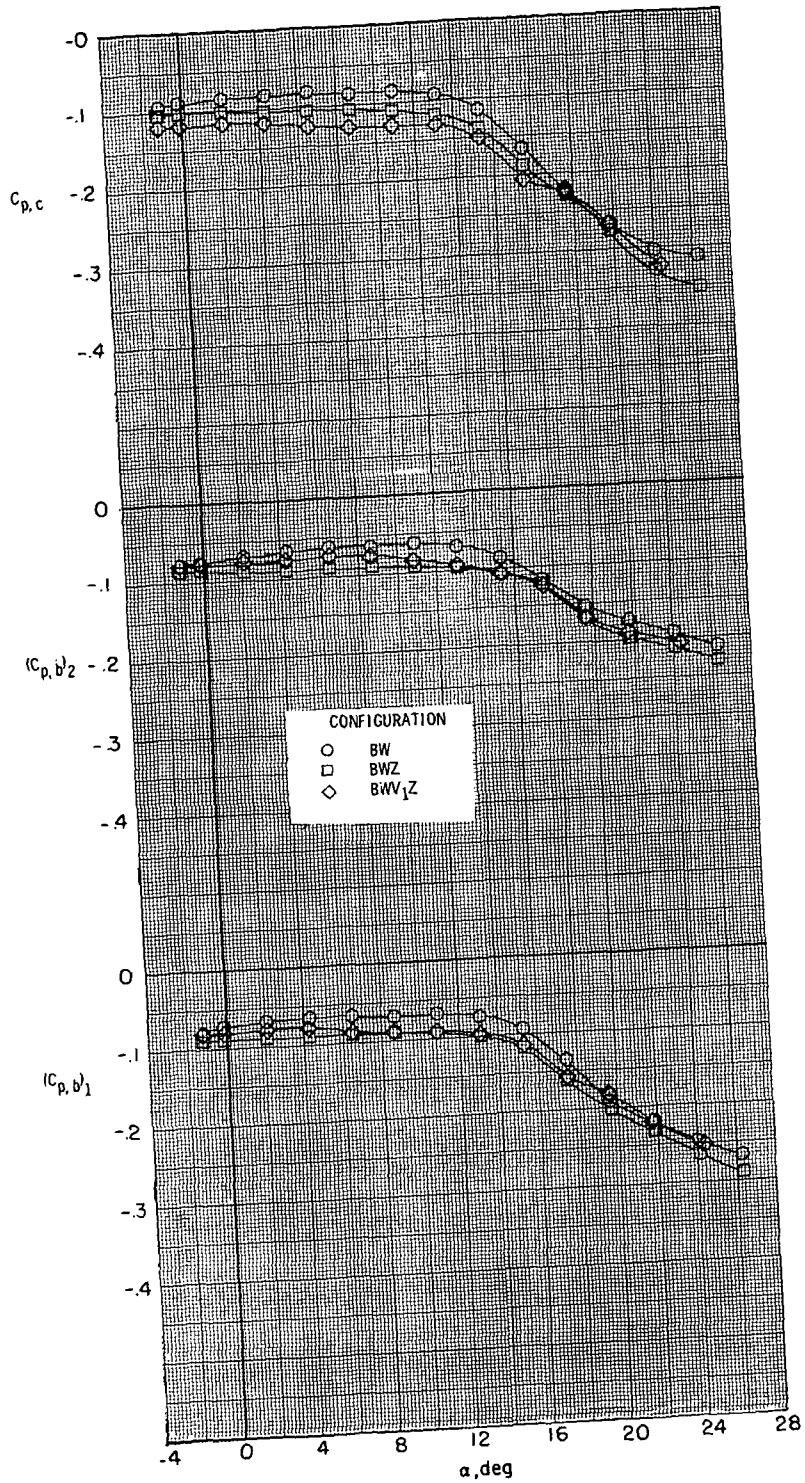

(e) $C_{p,b}$ and $C_{p,c}$ as a function of α.

Figure 10.- Concluded.

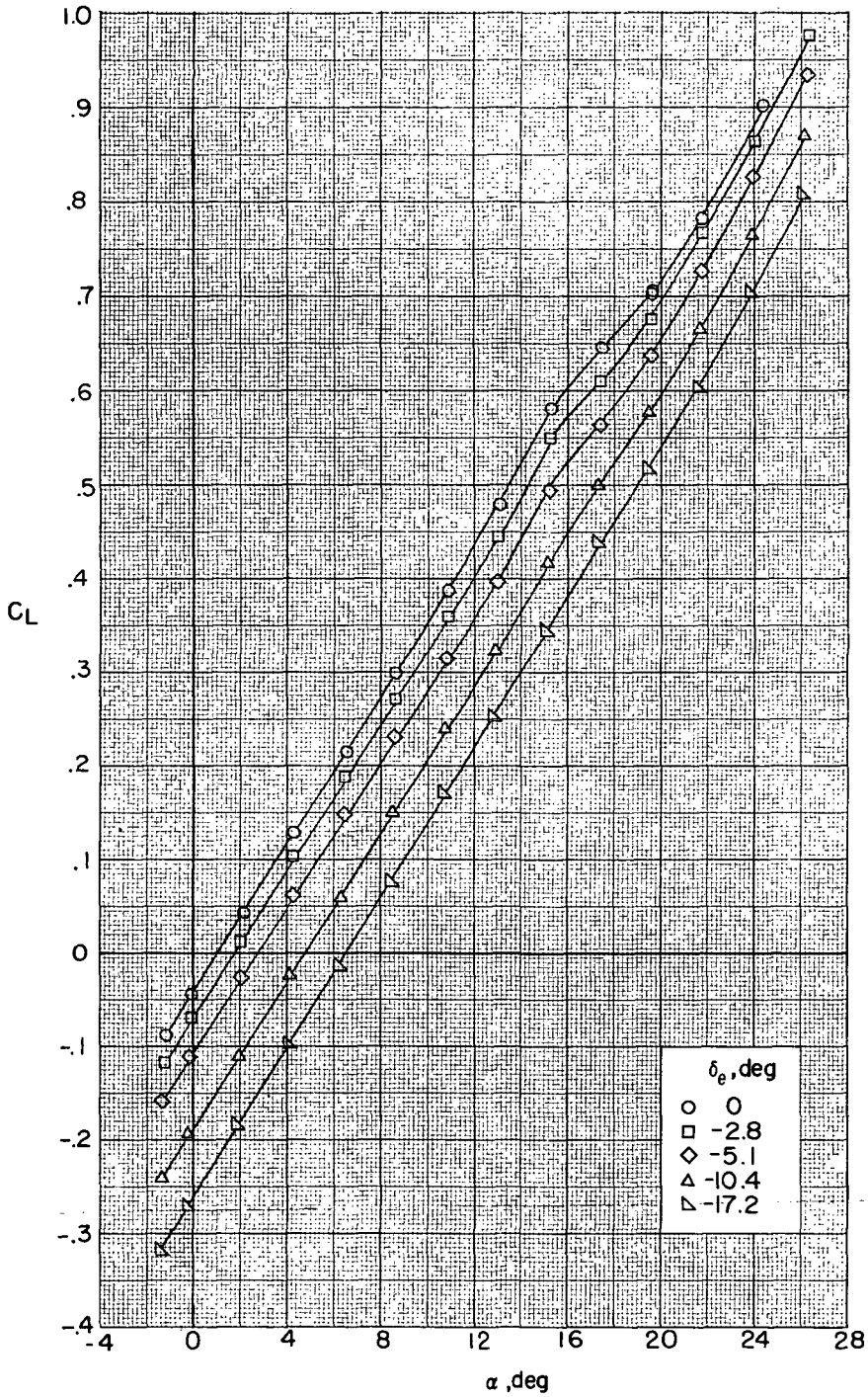

(a) C_L as a function of α.

Figure 11.- Longitudinal control effectiveness. $R = 21.0 \times 10^6$; BWV_1Z.

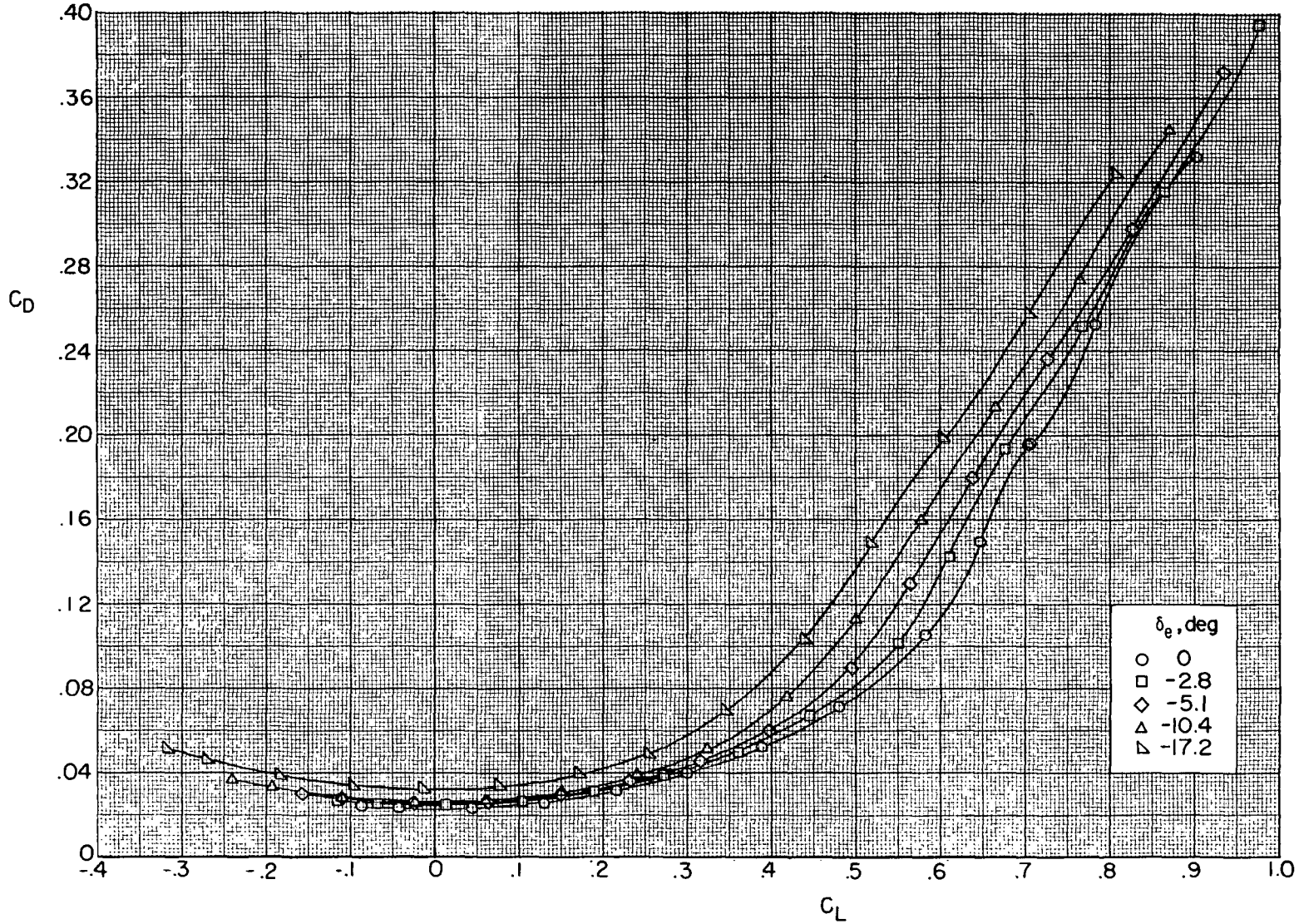

(b) C_D as a function of C_L.

Figure 11.- Continued.

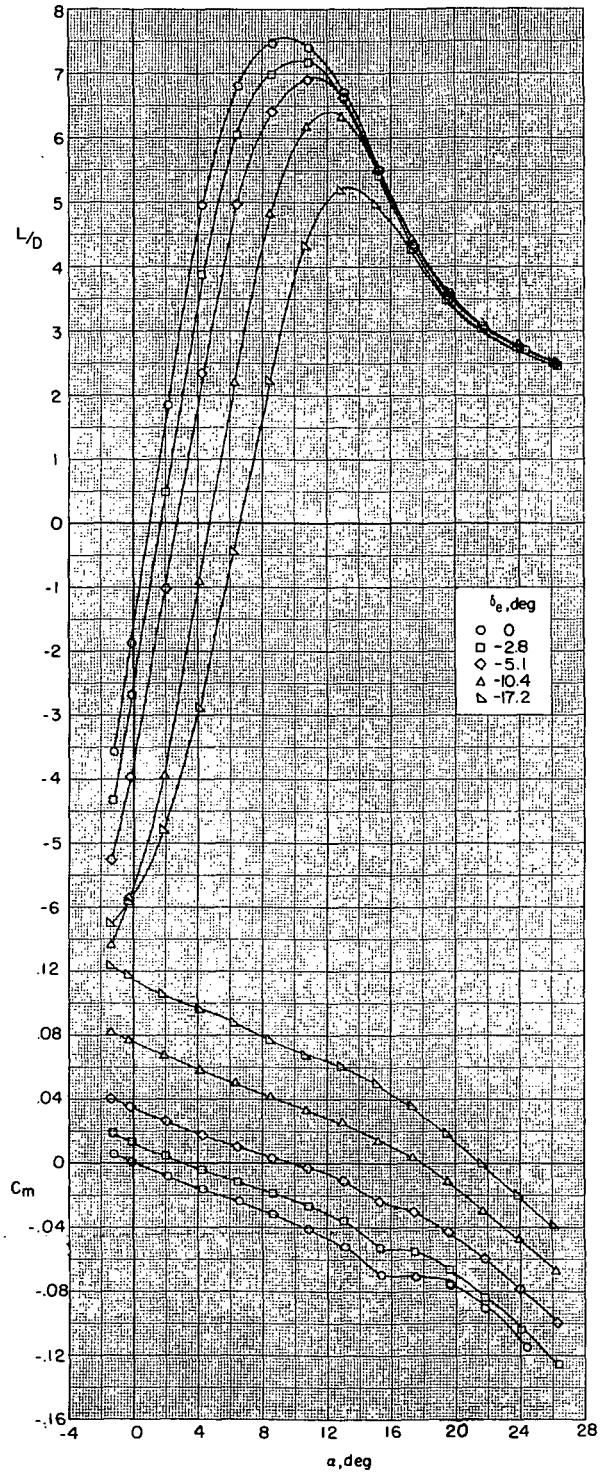

(c) C_m and L/D as a function of α.

Figure 11.- Continued.

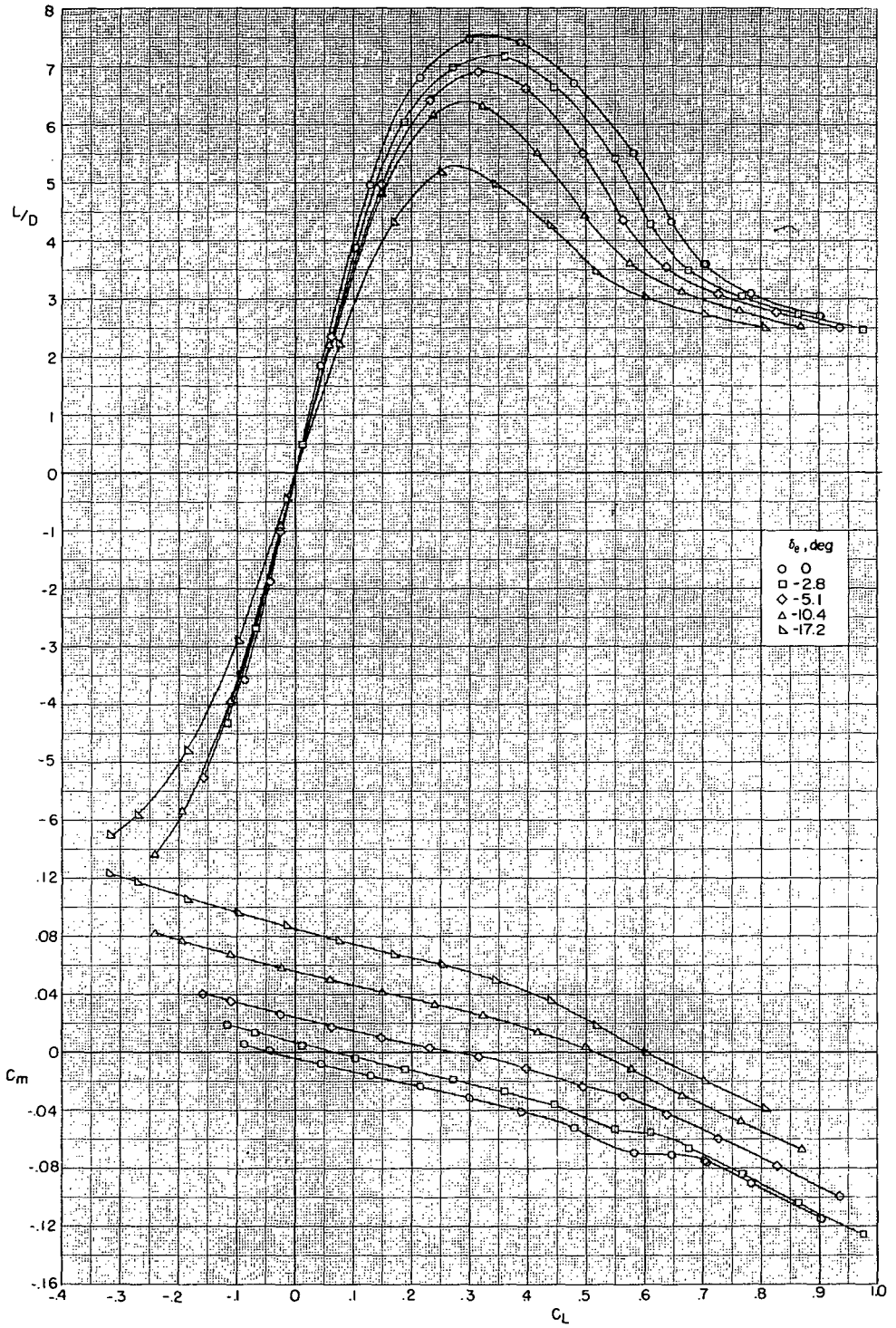

(d) C_m and L/D as a function of C_L.

Figure 11.- Continued.

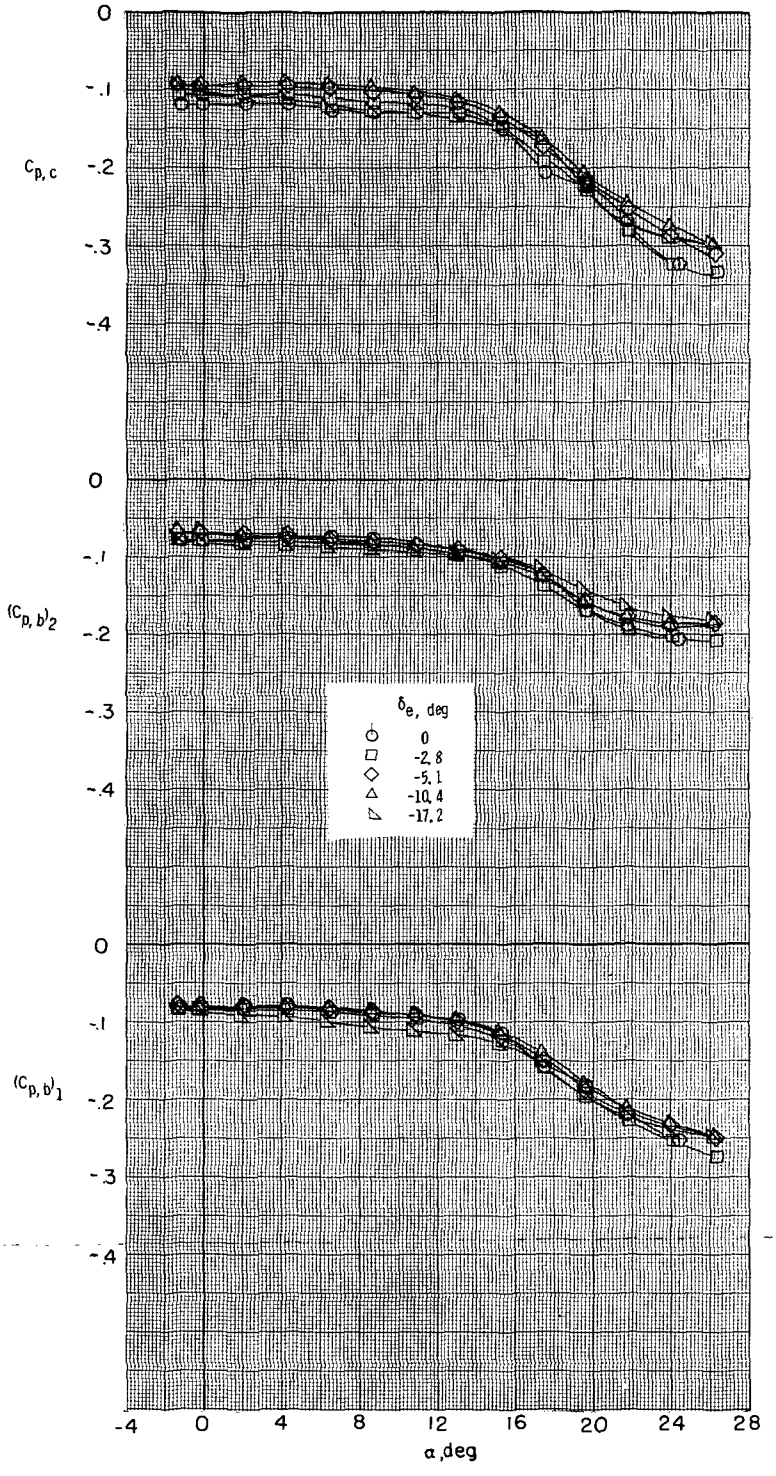

(e) $C_{p,b}$ and $C_{p,c}$ as a function of α.

Figure 11.- Concluded.

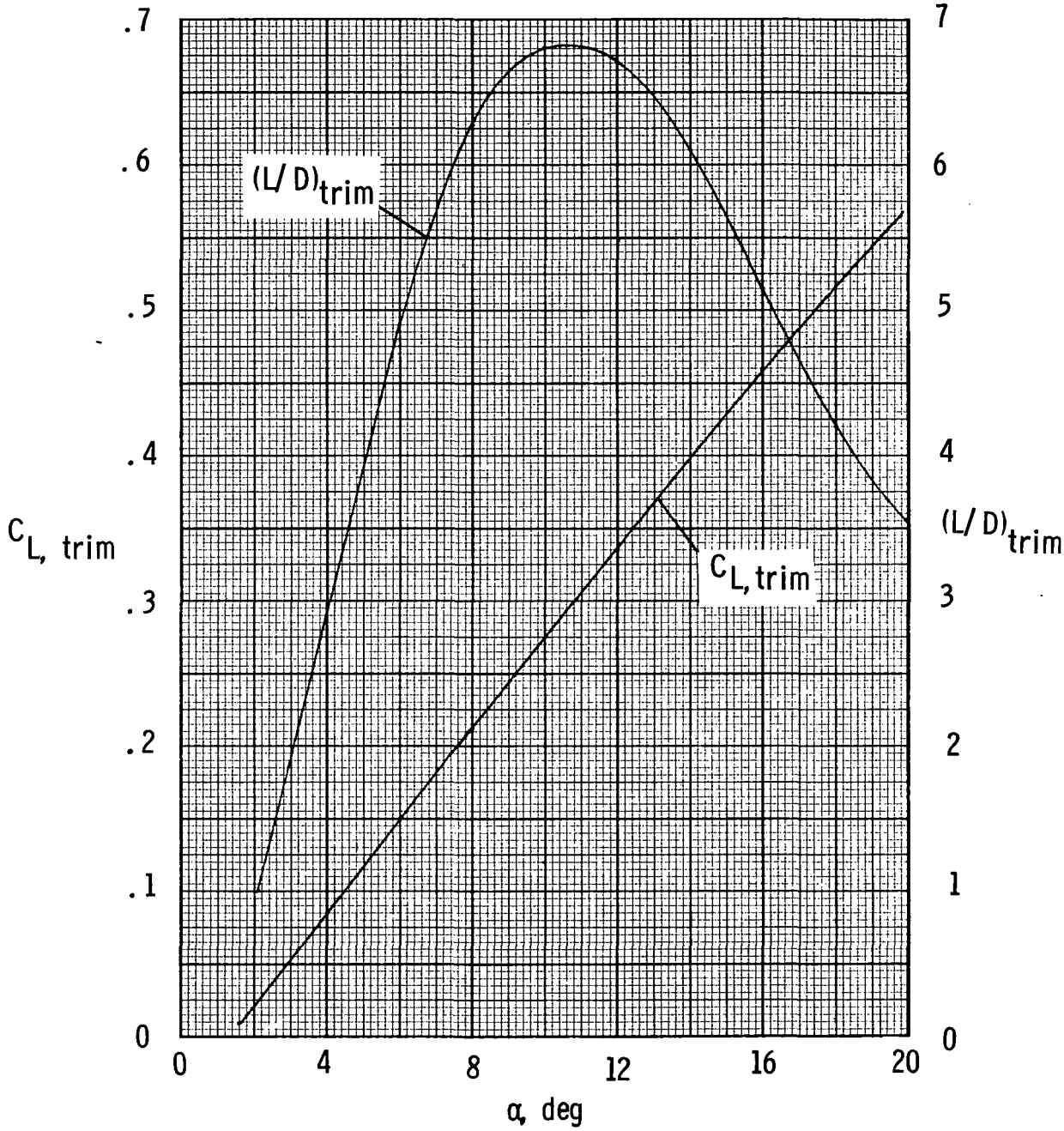

Figure 12.- Trim-performance characteristics of model. $R = 21.0 \times 10^6$.

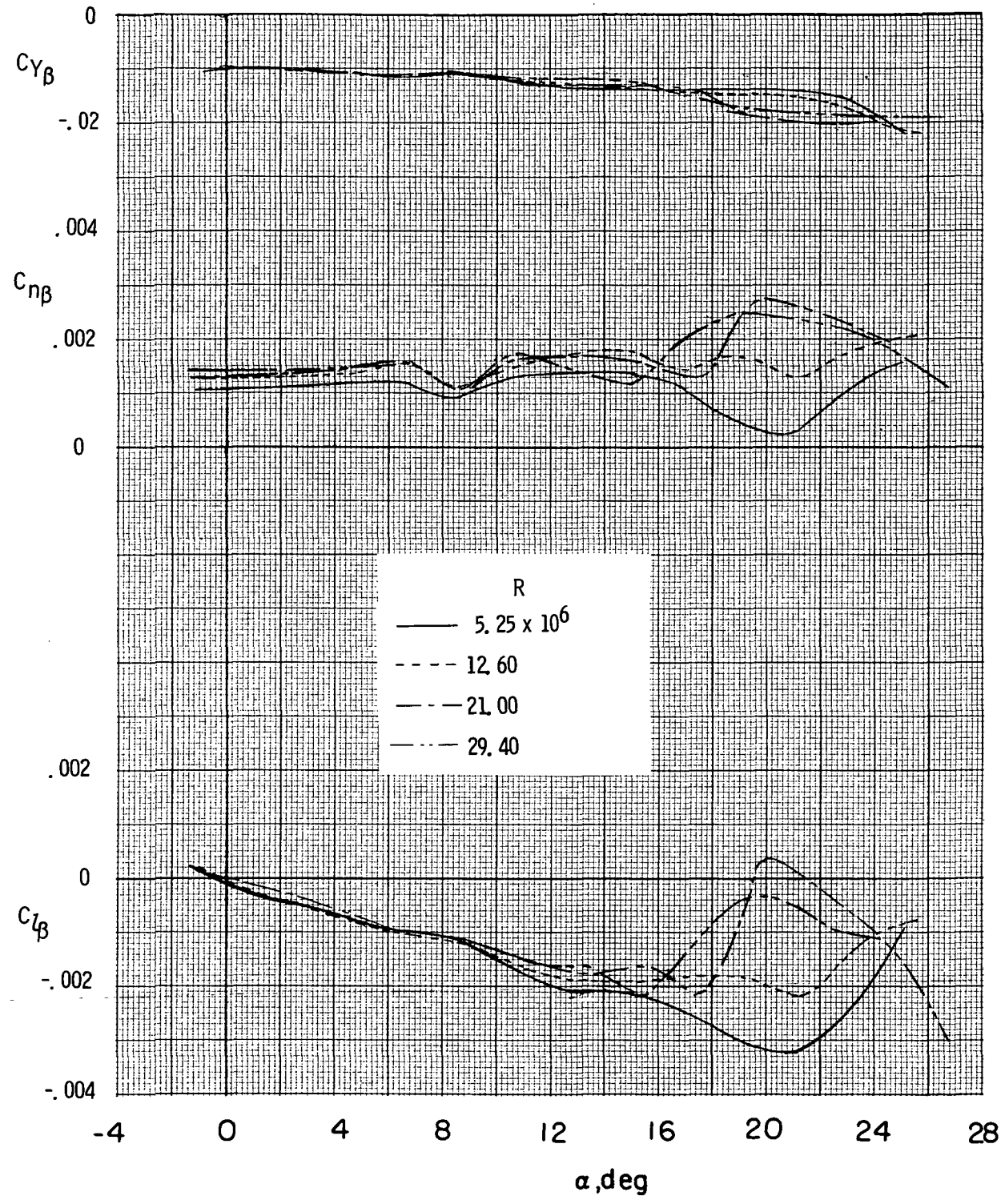

Figure 13.- Effect of Reynolds number on lateral-directional characteristics. $\delta_e = 0^o$.

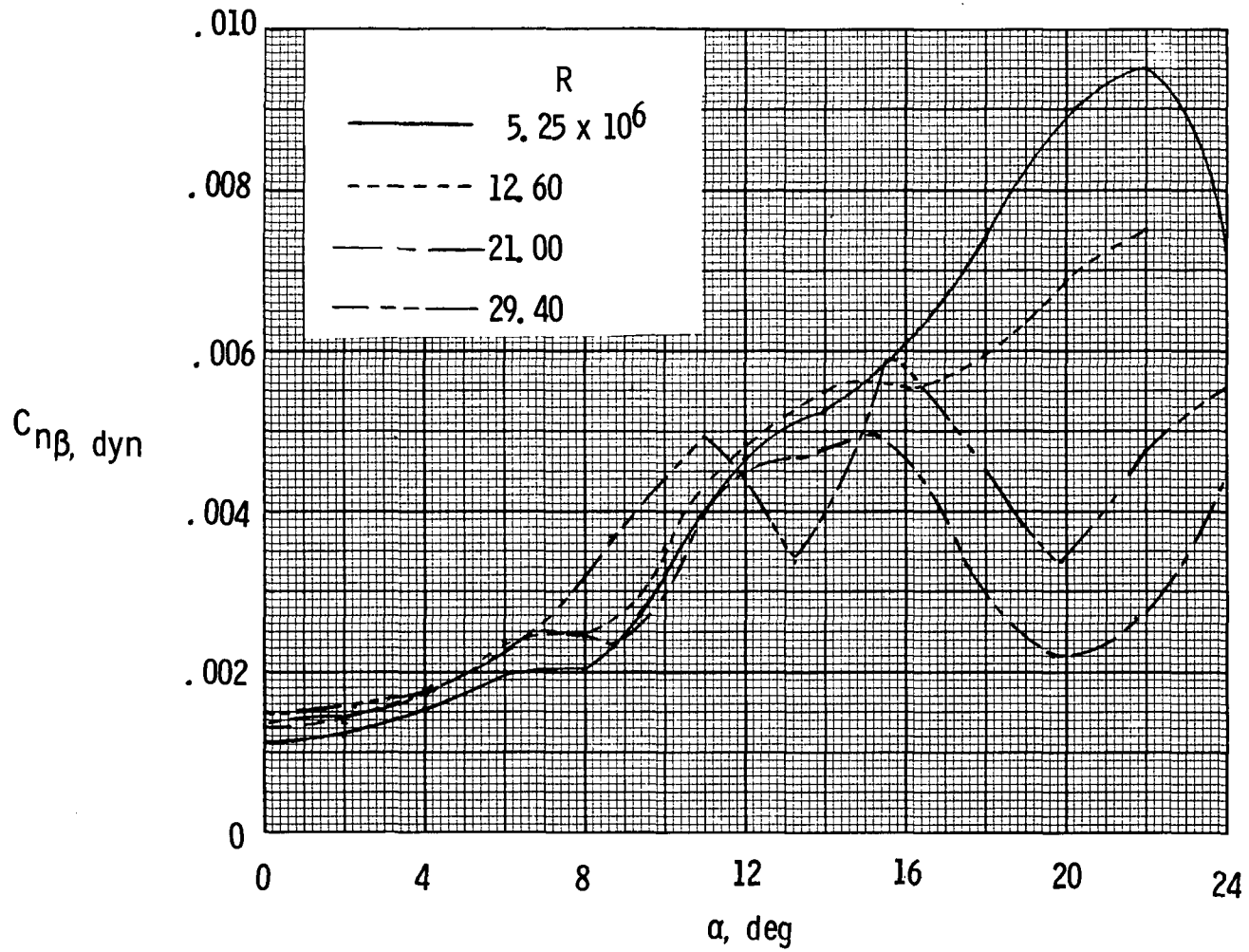

Figure 14.- Calculated values of $C_{n_{\beta,dyn}}$. $I_Z/I_X = 7.98$.

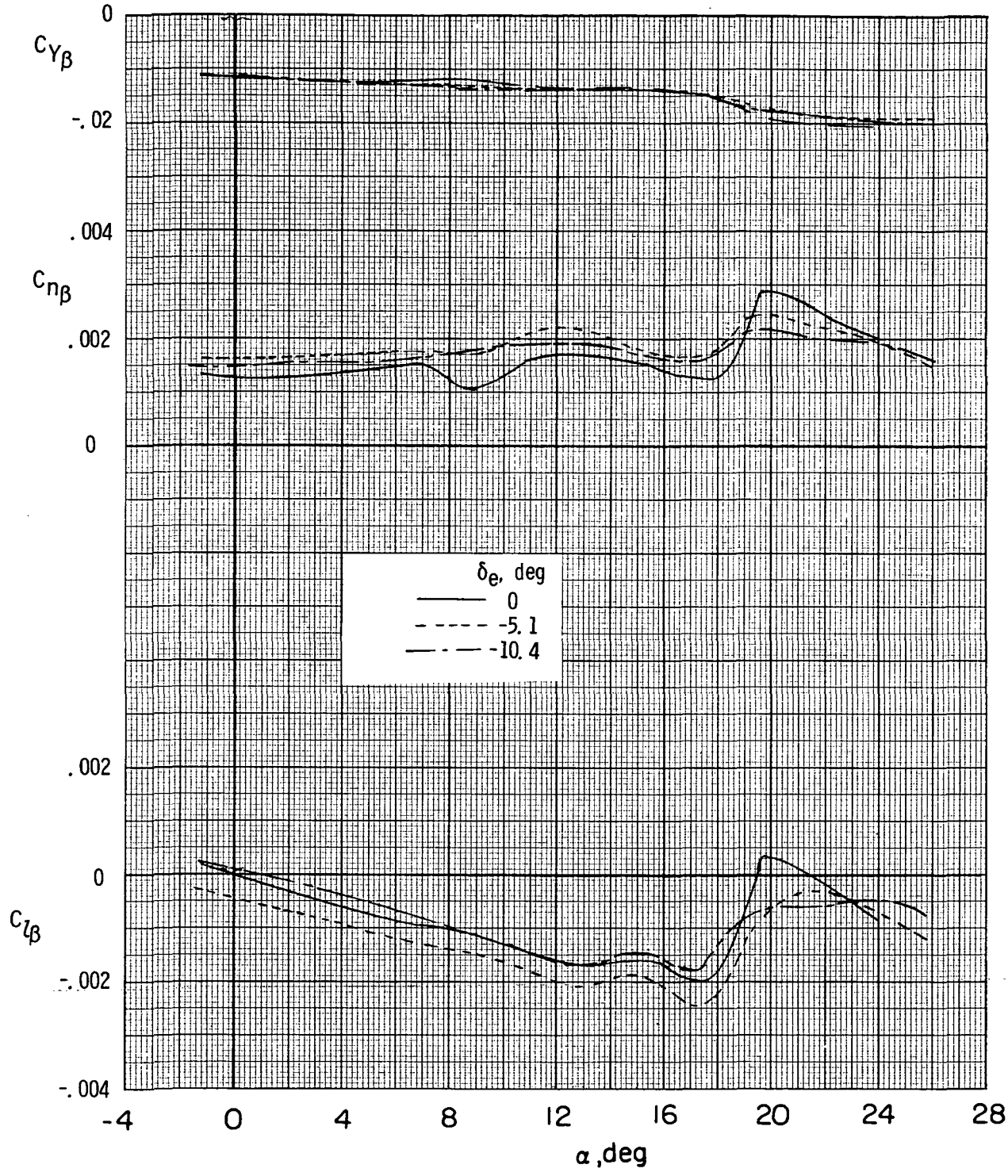

Figure 15.- Effect of pitch control on lateral-directional characteristics. $R = 21.0 \times 10^6$.

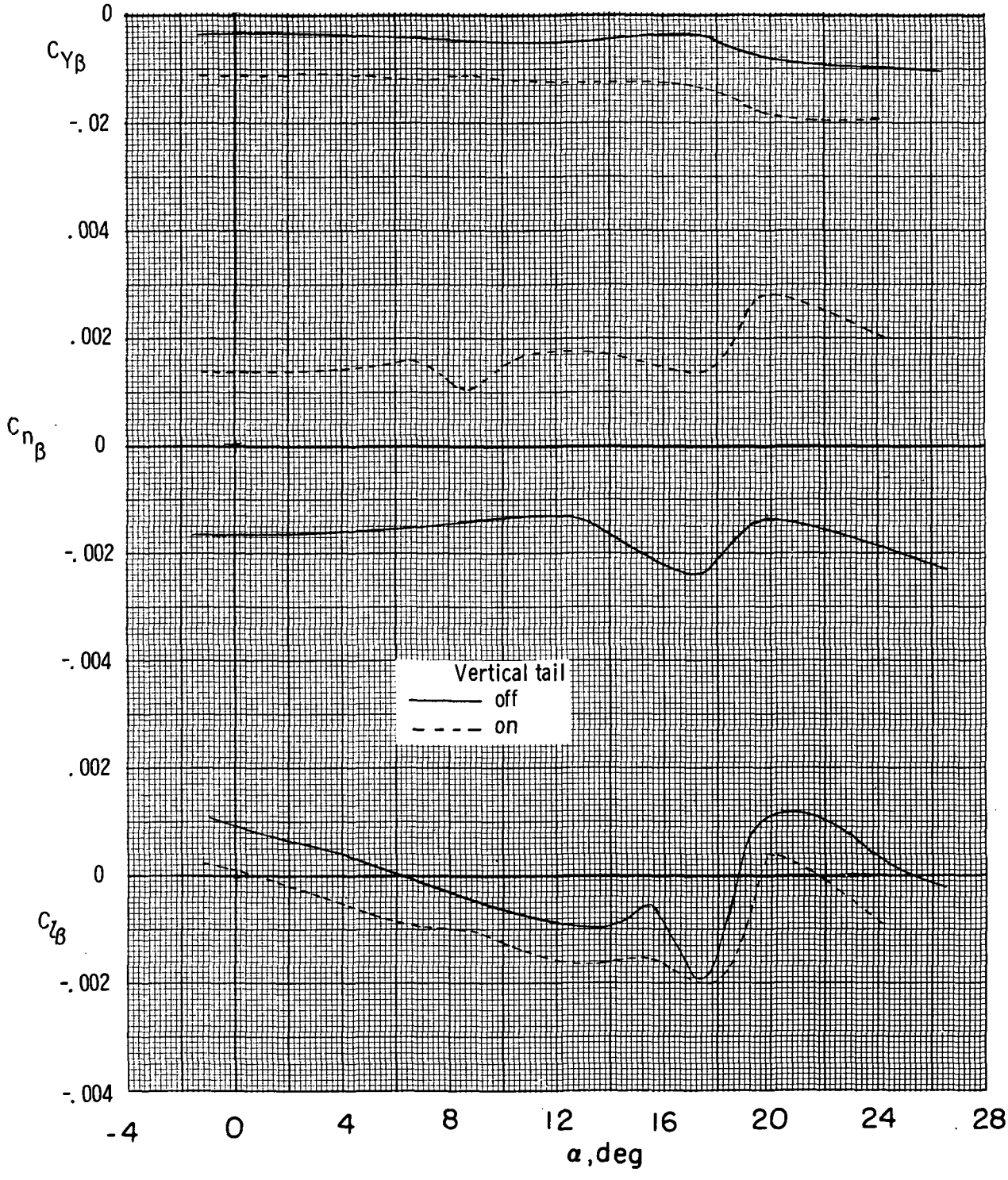

Figure 16.- Effect of vertical tail on lateral-directional characteristics. $\delta_e = 0^o$; $R = 21.0 \times 10^6$.

NATIONAL AERONAUTICS AND SPACE ADMINISTRATION
WASHINGTON, D.C. 20546

OFFICIAL BUSINESS
PENALTY FOR PRIVATE USE $300

SPECIAL FOURTH-CLASS RATE BOOK

POSTAGE AND FEES PAID
NATIONAL AERONAUTICS AND SPACE ADMINISTRATION
451

U.S.MAIL

POSTMASTER: If Undeliverable (Section 158 Postal Manual) Do Not Return

"The aeronautical and space activities of the United States shall be conducted so as to contribute . . . to the expansion of human knowledge of phenomena in the atmosphere and space. The Administration shall provide for the widest practicable and appropriate dissemination of information concerning its activities and the results thereof."

—NATIONAL AERONAUTICS AND SPACE ACT OF 1958

NASA SCIENTIFIC AND TECHNICAL PUBLICATIONS

TECHNICAL REPORTS: Scientific and technical information considered important, complete, and a lasting contribution to existing knowledge.

TECHNICAL NOTES: Information less broad in scope but nevertheless of importance as a contribution to existing knowledge.

TECHNICAL MEMORANDUMS: Information receiving limited distribution because of preliminary data, security classification, or other reasons. Also includes conference proceedings with either limited or unlimited distribution.

CONTRACTOR REPORTS: Scientific and technical information generated under a NASA contract or grant and considered an important contribution to existing knowledge.

TECHNICAL TRANSLATIONS: Information published in a foreign language considered to merit NASA distribution in English.

SPECIAL PUBLICATIONS: Information derived from or of value to NASA activities. Publications include final reports of major projects, monographs, data compilations, handbooks, sourcebooks, and special bibliographies.

TECHNOLOGY UTILIZATION PUBLICATIONS: Information on technology used by NASA that may be of particular interest in commercial and other non-aerospace applications. Publications include Tech Briefs, Technology Utilization Reports and Technology Surveys.

Details on the availability of these publications may be obtained from:

SCIENTIFIC AND TECHNICAL INFORMATION OFFICE

NATIONAL AERONAUTICS AND SPACE ADMINISTRATION

Washington, D.C. 20546